

# Level attraction from interference in two-tone driving

Alan Gardin,<sup>1,2,\*</sup> Guillaume Bourcin,<sup>2</sup> Christian Person,<sup>2</sup> Christophe Fumeaux,<sup>3</sup>  
Romain Lebrun,<sup>4</sup> Isabella Boventer,<sup>4</sup> Giuseppe C. Tettamanzi,<sup>5</sup> and Vincent Castel<sup>2</sup>

<sup>1</sup>*School of Physics, The University of Adelaide, Adelaide SA 5005, Australia*

<sup>2</sup>*IMT Atlantique, Lab-STICC, UMR CNRS 6285, F-29238 Brest, France*

<sup>3</sup>*School of Electrical Engineering and Computer Science,*

*The University of Queensland, Brisbane QLD 4072, Australia*

<sup>4</sup>*Unité Mixte de Physique, CNRS, Thales, Université Paris-Saclay, 91767 Palaiseau, France*

<sup>5</sup>*School of Chemical Engineering and Advanced Materials,  
The University of Adelaide, Adelaide SA 5005, Australia*

Coherent and dissipative couplings, respectively characterised by energy level repulsion and attraction, each have different applications for quantum information processing. Thus, a system in which both coherent and dissipative couplings are tunable on-demand and in-situ is tantalising. A first step towards this goal is the two-tone driving of two bosonic modes, whose experimental signature was shown to exhibit controllable level repulsion and attraction by changing the phase and amplitude of one drive. However, whether the underlying physics is that of coherent and dissipative couplings has not been clarified, and cannot be concluded solely from the measured resonances (or anti-resonances) of the system. Here, we show how the physics at play can be analysed theoretically. Combining this theory with realistic finite-element simulations, we deduce that the observation of level attraction originates from interferences due to the measurement setup, and not dissipative coupling. Beyond the clarification of a novel origin for level attraction attributed to interference, our work demonstrates how effective Hamiltonians can be derived to appropriately describe the physics.

*Introduction.* The coherent coupling between two systems corresponds to the coherent exchange of energy between them, and is characterised by energy level repulsion (also known as normal-mode splitting or an anti-crossing). This phenomenon is ubiquitous in physics, spanning the classical coupling of two harmonic oscillators [1] to the coupling of bosonic quasi-particles with two-level systems [2] or other bosonic excitations [3]. With respect to quantum information processing, coherent coupling allows to convert quantum information between light and solid state degrees of freedom, and is therefore an elementary building-block of quantum communication [4–6]. On the other hand, dissipative coupling [7–9], characterised by energy level attraction instead, arises due to the indirect coupling of two modes mediated by a common reservoir [10–12] (e.g. a strongly dissipative auxiliary mode [13], a photonic environment [14–16], metallic leads [17]). The merging of energy levels characterising dissipative couplings leads to exceptional points [18–21], which can be useful for topological energy transfer [22], and improved sensitivity for quantum metrology and quantum sensing applications [23, 24]. Furthermore, balancing coherent and dissipative couplings, using dissipation engineering and synthetic gauge fields, allows to break time-reversal symmetry and thus create non-reciprocal devices [10–12, 25–28]. Therefore, building a system in which both coherent and dissipative couplings co-exist and are tunable would be useful to access all the aforementioned applications in a unique versatile platform.

Such a system, due to the presence of both coherent and dissipative couplings, should have an energy spectrum exhibiting both level repulsion and level attrac-

tion. Two reflection experiments [29, 30], in which two coherently-coupled bosonic modes were simultaneously driven, suggested such an energy level structure (and hence the presence of coherent and dissipative couplings). Indeed, it is usually expected that the response of a system to excitations at frequencies close to their normal modes leads to resonances (or anti-resonances), with various possible line shapes informing on the underlying physics [31, 32]. However, inspection of the experimental signature alone is not sufficient because it may not be related to the energy levels. Additionally, while dissipative coupling implies level attraction in a variety of platforms such as optomechanics [33], Aharonov-Bohm interferometers [17] or semiconductor microcavities [16] and micropillar lasers [34], alternative physics can also lead to level attraction, as exemplified in optomechanics [35] or spinor condensates [36]. For all these reasons, the physics at play in two-tone driving remains unclear.

In this letter, we model a two-tone driving experiment, similar to those of [29, 30]. Our starting point is the Hamiltonian of two coherently coupled bosonic modes, whose spectrum is that of level repulsion. To model the two-tone driving and the experimentally accessible quantities, we use quantum Langevin equations (QLEs) and the input-output formalism [37]. This theoretical treatment allows to find an analytical expression for the experimental signature, where both level repulsion and attraction can occur. Importantly, we show analytically and using finite element simulations, that level attraction can be attributed to an anti-resonance due to the destructive interference between the reflection and transmission coefficients. To clarify the physics, we derive the open-system effective Hamiltonian of the two-tone driven system, and

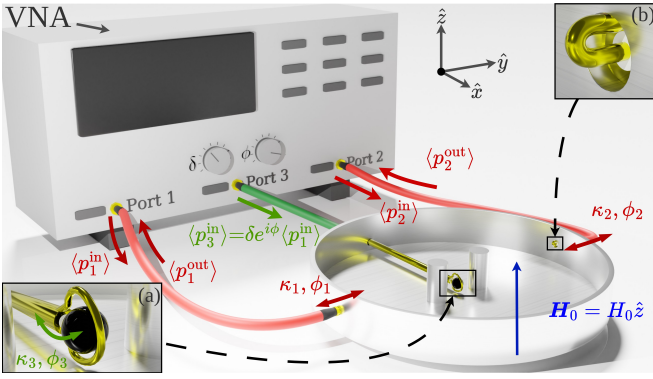


FIG. 1. Schematic of a two-tone driving experiment using a two-post re-entrant cavity [38] loaded with a ferromagnetic sphere made of Yttrium-Iron-Garnet. Ports 1 and 3 are always active and drive respectively the cavity and magnon modes. The cavity is connected to a vector network analyser (VNA) to measure the reflection at Port 1 and the transmission through Port 2. Inset (a): the YIG sphere is placed at the centre of a loop made by soldering the inner and outer conductor of a coaxial cable, itself placed between the two posts where the cavity mode's magnetic field is strongest. In the picture, the loop is in the  $(x, z)$  plane, and the YIG sphere is biased along  $\hat{z}$  by the static magnetic field  $\mathbf{H}_0$ . Inset (b): antenna used to excite the cavity modes.

show that the physics remains exclusively that of coherent coupling, despite the observation of level attraction.

*Quantum Langevin equations.* We consider the experimental setup of fig. 1, where a ferromagnetic sphere made of Yttrium-Iron-Garnet (YIG) is placed inside a microwave cavity. The second-quantised Hamiltonian of the system enclosed inside the cavity is that of the lowest-order magnon mode (quantised spin wave) coupled to a single cavity mode, described by [9]

$$H_{\text{sys}} = \hbar\omega_c c^\dagger c + \hbar\omega_m m^\dagger m + \hbar(gcm^\dagger + g^*c^\dagger m), \quad (1)$$

where  $g/2\pi$  is the (complex) coherent coupling strength [39, 40] between the cavity mode (operators  $c, c^\dagger$ ) and the magnon mode (operators  $m, m^\dagger$ ). The frequency of the cavity mode  $\omega_c/2\pi$  is fixed by the cavity's geometry, while the ferromagnetic resonance of the magnon is tuned by a static magnetic field  $\mathbf{H}_0 = H_0\hat{z}$  as  $\omega_m = \gamma|\mathbf{H}_0|$  where  $\gamma/2\pi = 28$  GHz/T is the gyromagnetic ratio.

The quantum Langevin equations (QLEs) allow to model the coupling of the cavity system described by eq. (1) to the environment, to model intrinsic dissipation or external drives. To model the intrinsic damping of the cavity mode  $c$  and the magnon mode  $m$ , we assume that they each couple to their own bosonic bath with coupling constants  $\kappa_c/2\pi$  and  $\kappa_m/2\pi$ . As per fig. 1, the cavity system described by eq. (1) is coupled to three ports  $p_i$ , labelled from 1 to 3, where the first two ports couple only to the cavity mode (with real-valued coupling constants  $\kappa_1/2\pi$  and  $\kappa_2/2\pi$  and phases  $\phi_1, \phi_2$  [41]) and the third couples only to the magnon mode (real-valued

coupling constant  $\kappa_3/2\pi$  with phase  $\phi_3$ ). Physically, the coupling of the magnon to port 3 is due to the Zeeman interaction with the magnetic field created by the loop of port 3. The QLE for the cavity and magnon modes then read [42]

$$\dot{c} = -i\tilde{\omega}_c c - ig^* m - \sqrt{\kappa_c} c^{\text{in}} - \sqrt{\kappa_1} e^{i\phi_1} p_1^{\text{in}} - \sqrt{\kappa_2} e^{i\phi_2} p_2^{\text{in}}, \quad (2)$$

$$\dot{m} = -i\tilde{\omega}_m m - igc - \sqrt{\kappa_m} m^{\text{in}} - \sqrt{\kappa_3} e^{i\phi_3} p_3^{\text{in}} \quad (3)$$

where  $\tilde{\omega}_c = \omega_c - i\frac{\kappa_c + \kappa_1 + \kappa_2}{2}$  and  $\tilde{\omega}_m = \omega_m - i\frac{\kappa_m + \kappa_3}{2}$ . In the QLEs,  $c^{\text{in}}$  and  $m^{\text{in}}$  account for intrinsic damping and have zero mean  $\langle c^{\text{in}} \rangle = \langle m^{\text{in}} \rangle = 0$ , while  $p_i^{\text{in}}$  represent the coupling to the ports.

*Two-tone reflection and transmission.* We now assume that  $p_1^{\text{in}}$  and  $p_3^{\text{in}}$  correspond to coherent drives at the same frequency, albeit with a phase and amplitude difference written  $\langle p_3^{\text{in}} \rangle = \delta e^{i\phi} \langle p_1^{\text{in}} \rangle$ . We also perform a semi-classical approximation and neglect quantum fluctuations, which amounts to only considering expectation values. Using the input-output formalism [42], the reflection at Port 1 when Port 3 is active is found to be

$$r_1(\omega) = \frac{\langle p_1^{\text{out}} \rangle |_{\langle p_2^{\text{in}} \rangle = 0}}{\langle p_1^{\text{in}} \rangle} \quad (4)$$

$$= 1 - i\sqrt{\kappa_1} \frac{\tilde{\Delta}_m \sqrt{\kappa_1} + g^* \sqrt{\kappa_3} e^{i(\phi_3 - \phi_1)} \delta e^{i\phi}}{\tilde{\Delta}_c \tilde{\Delta}_m - |g|^2} \quad (5)$$

where  $\tilde{\Delta}_c = \omega - \tilde{\omega}_c$  and  $\tilde{\Delta}_m = \omega - \tilde{\omega}_m$ . By comparing with the expressions of the standard S-parameters [42], we note that the reflection  $r_1$  can also be written  $r_1(\omega) = S_{11} + \delta e^{i\phi} S_{13}$  which is expected given the linearity of the problem.

For  $\delta \neq 0$ , the reflection coefficient  $r_1$  can be greater than one, because it is only normalised to the input power from Port 1, thus neglecting that of Port 3. Following the setup of fig. 1, and taking the power out of Port 1 as a reference, the VNA outputs a power  $1 + \delta^2$ , so we can renormalise the reflection to  $R_1(\omega) = \frac{1}{\sqrt{1 + \delta^2}} r_1(\omega)$ . Similarly, we can calculate the normalised transmission coefficient through Port 2 when both Port 1 and Port 3 are active, and we find [43]

$$T_2(\omega) = \frac{1}{\sqrt{1 + \delta^2}} \frac{\langle p_2^{\text{out}} \rangle |_{\langle p_2^{\text{in}} \rangle = 0}}{\langle p_1^{\text{in}} \rangle} = \frac{S_{21} + \delta e^{i\phi} S_{23}}{\sqrt{1 + \delta^2}}. \quad (6)$$

We plot  $|R_1|$  in fig. 2 and  $|T_2|$  in fig. 3 with the parameters  $\omega_c/2\pi = 10$  GHz,  $|g|/2\pi = 20$  MHz,  $\kappa_c/2\pi = \kappa_m/2\pi = 1$  MHz,  $\kappa_1/2\pi = \kappa_2/2\pi = 10$  MHz,  $\kappa_3/2\pi = 5$  MHz,  $\varphi = -\pi/2$  and  $\phi_1 = \phi_2 = \phi_3 = 0$ . The reflection  $R_1$  exhibits controllable level repulsion and attraction depending on the amplitude  $\delta$  of the drives and the dephasing  $\phi$ , mirroring the experimental results of [29, 30]. On the other hand, we notice that the transmission  $T_2$  only shows level repulsion, despite the system being driven in

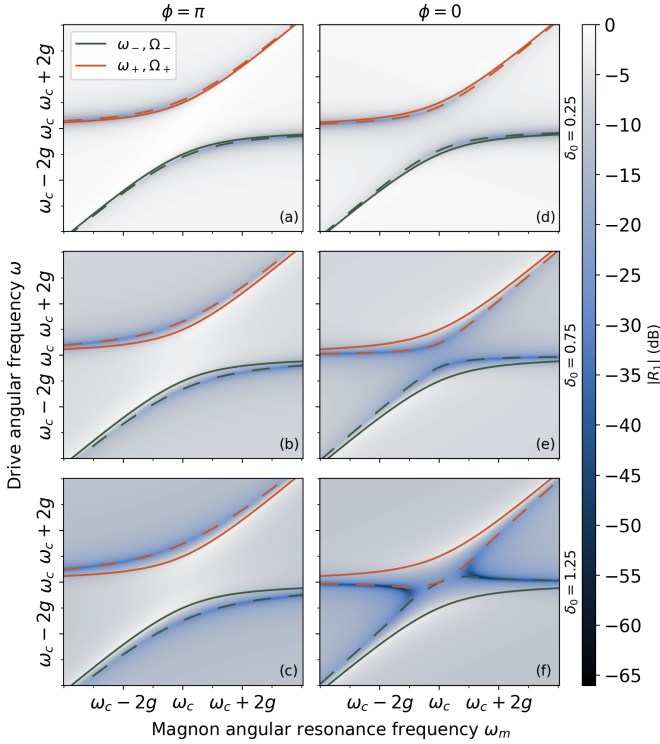


FIG. 2. Normalised reflection amplitude  $|R_1|$  at Port 1 for increasing values of  $\delta_0 = \frac{\sqrt{\kappa_1 \kappa_3}}{|g|} \delta$  from top to bottom, and a dephasing  $\phi = \pi$  (first column) and  $\phi = 0$  (second column) between the drives of Port 1 and Port 3. The solid lines correspond to the real part of the zeros  $\tilde{\omega}_\pm$  of the denominator of  $R_1$ , given by eq. (9), while the dashed lines correspond to the zeros  $\tilde{\Omega}_\pm$  of the nominator of  $R_1$ .

exactly the same way: between  $R_1$  and  $T_2$ , only the measurement location changes, and thus the physics should be the same.

*Analysis of the two-tone reflection coefficient.* An advantage of the input-output formalism is that it allows us to understand analytically the spectral features of fig. 2. Indeed, by writing  $r_1(\omega) = N(\omega)/D(\omega)$  in terms of a nominator  $N$  and a denominator  $D$ , the denominator can be factorised as

$$D(\omega) = \omega^2 - (\tilde{\omega}_c + \tilde{\omega}_m)\omega + \tilde{\omega}_c \tilde{\omega}_m - |g|^2 \quad (7)$$

$$= (\omega - \tilde{\omega}_+)(\omega - \tilde{\omega}_-) \quad (8)$$

where

$$\tilde{\omega}_\pm = \frac{\tilde{\omega}_c + \tilde{\omega}_m}{2} \pm \frac{\sqrt{(\tilde{\omega}_c - \tilde{\omega}_m)^2 + 4|g|^2}}{2} \quad (9)$$

are the complex-valued solutions of the quadratic eq. (7).

On the other hand, the nominator  $N$  can be written as

$$N(\omega) = \omega^2 - (\tilde{\omega}'_c + \tilde{\omega}_m)\omega + \tilde{\omega}'_c \tilde{\omega}_m - G^2 \quad (10)$$

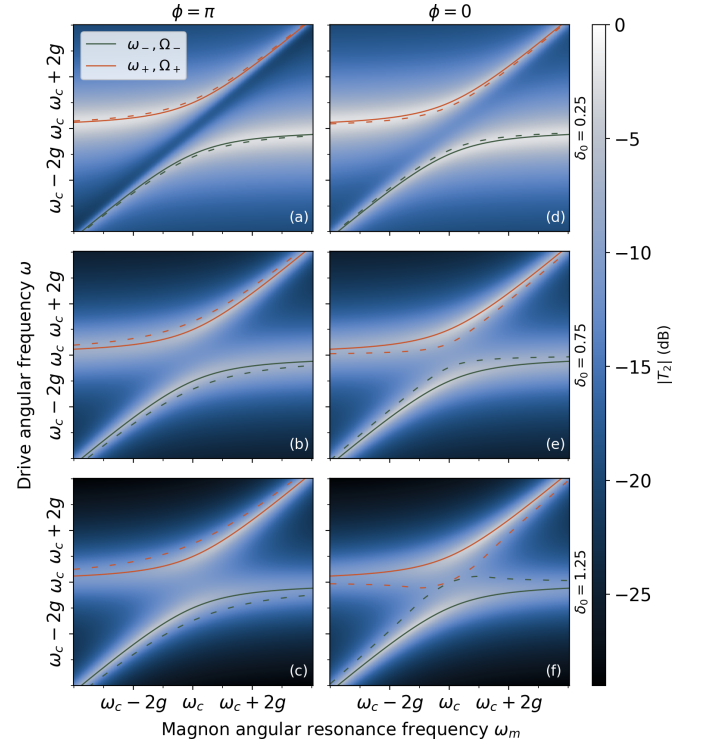


FIG. 3. Normalised transmission amplitude  $|T_2|$  through Port 2 for  $\phi = \pi$  and  $\phi = 0$ , and increasing values of  $\delta_0$  from top to bottom. The parameters used are identical to those of fig. 2.

where we defined  $\tilde{\omega}'_c = \tilde{\omega}_c + i\kappa_1$  and

$$G = |g| \sqrt{1 + \frac{\sqrt{\kappa_1 \kappa_3}}{|g|} \delta e^{i(\phi + \phi_3 - \phi_1 + \frac{\pi}{2} - \arg g)}}, \quad (11)$$

with  $\arg g$  is the phase of the complex number  $g$ . Comparing eqs. (7) and (10), we see that the nominator can be factored similarly to the denominator as  $N(\omega) = (\omega - \tilde{\Omega}_+(\delta, \phi))(\omega - \tilde{\Omega}_-(\delta, \phi))$ , where the complex frequencies  $\tilde{\Omega}_\pm(\delta, \phi)$  are formally identical to eq. (9), after replacing  $\omega_c \mapsto \omega'_c$  and  $|g| \mapsto G$ . Finally, we obtain

$$r_1(\omega) = \frac{(\omega - \tilde{\Omega}_+(\delta, \phi))(\omega - \tilde{\Omega}_-(\delta, \phi))}{(\omega - \tilde{\omega}_+)(\omega - \tilde{\omega}_-)}. \quad (12)$$

For small dissipation rates  $\kappa_i$ , the imaginary part of  $\tilde{\omega}_\pm$  is small compared to its real part. Therefore, in eq. (12), when  $\omega$  is close to  $\omega_\pm = \text{Re}\{\tilde{\omega}_\pm\}$ , the denominator  $|D|$  of  $|R_1|$  almost vanishes, leading to a resonance behaviour (maxima) of  $|R_1|$ . Furthermore,  $\omega_\pm$  correspond to the spectrum of the Hamiltonian of eq. (1), and hence this resonance behaviour is expected to give information about the spectrum of the closed-system. As shown by the solid lines in figs. 2 and 3, the spectrum is that of coherent coupling, characterised by energy level repulsion with an angular frequency gap  $2|g|$ . Hence, the denominator of  $|R_1|$ , or equivalently its resonances, does inform on the underlying physics.

The situation is different for the nominator  $N$  of  $R_1$ . Indeed, while the expressions of  $\tilde{\omega}_\pm$  and  $\tilde{\Omega}_\pm$  are formally identical, the effective coupling strength  $G/2\pi$  for  $\tilde{\Omega}_\pm$  is complex-valued (while it is real-valued,  $|g|/2\pi$ , for  $\tilde{\omega}_\pm$ ) which can lead to level attraction. To see this more clearly, it is convenient to introduce the effective amplitude  $\delta_0 = \frac{\sqrt{\kappa_1\kappa_3}}{|g|}\delta$  and the effective phase  $\phi_0 = \phi_1 - \phi_3 + \arg g - \frac{\pi}{2}$  of Port 3. We can then rewrite eq. (11) as

$$G = g\sqrt{1 + \delta_0 e^{i(\phi - \phi_0)}}. \quad (13)$$

Therefore, when  $\phi - \phi_0 = 0$  the effective coupling strength  $G/2\pi$  is real-valued and increases as  $\delta_0$  increases, leading to an increase of level repulsion (see the dashed lines in the first column of fig. 2). On the other hand, when  $\phi - \phi_0 = \pi$ , the effective coupling strength is real-valued when  $\delta_0 < 1$  and diminishes when  $\delta_0$  increases. Eventually, when  $\delta_0 > 1$ , the coupling strength becomes purely imaginary due to taking the square root of a negative number, leading to level attraction. In the limiting case where  $\delta_0 = 1$ , we have  $G = 0$  and we obtain two uncoupled anti-resonances (an horizontal one at the cavity mode frequency and a diagonal one at the magnon's frequency  $\omega_m/2\pi$ ). As can be seen from the dashed lines in fig. 2, these spectral features indeed correspond to anti-resonances (zeros of the nominator  $N$  corresponding to minima of  $|R_1|$ ) at the frequencies  $\Omega_\pm$ . Physically, these frequencies  $\Omega_\pm$  are determined by the interference between the nominators of  $S_{11}$  and  $S_{13}$  since  $r_1(\omega) = S_{11} + \delta e^{i\phi} S_{13}$ . Hence, the input-output formalism shows that while the denominator of  $|R_1|$  informs on the physics, the nominator is interference-based. Indeed, the denominator of both  $R_1$  and  $T_2$  are identical, leading to similar resonant behaviour following the coherent coupling spectrum. However, their anti-resonance behaviours differ because their nominators differ [43].

*Numerical finite element results.* The input-output formalism provides interesting insights thanks to the resulting analytical expressions. However, it remains a toy-model of a two-tone driving experiment. Instead, a realistic modelling, taking into account the geometry of the cavity and of the ports, can be performed using COMSOL Multiphysics<sup>®</sup>, a finite element modelling software. We use a two-post re-entrant cavity [44, 45], similar to that sketched in fig. 1, in which the loop antenna of Port 3 is inserted from the bottom of the cavity [46]. At the location of the YIG sphere, the cavity mode's magnetic field is purely along the  $\hat{x}$  axis [38]. In our analysis, we assumed that Port 3 does not couple to the cavity mode, which requires us to orient the loop antenna so that it generates a magnetic field orthogonal to the cavity mode. Thus, noting  $\hat{\mathbf{n}}$  the normal to the plane of the loop, we need  $\hat{\mathbf{n}}$  to be in the  $(x, z)$  plane. Furthermore, since only the components orthogonal to the static magnetic field  $H_0\hat{\mathbf{z}}$  contribute to the coupling between Port 3 and the

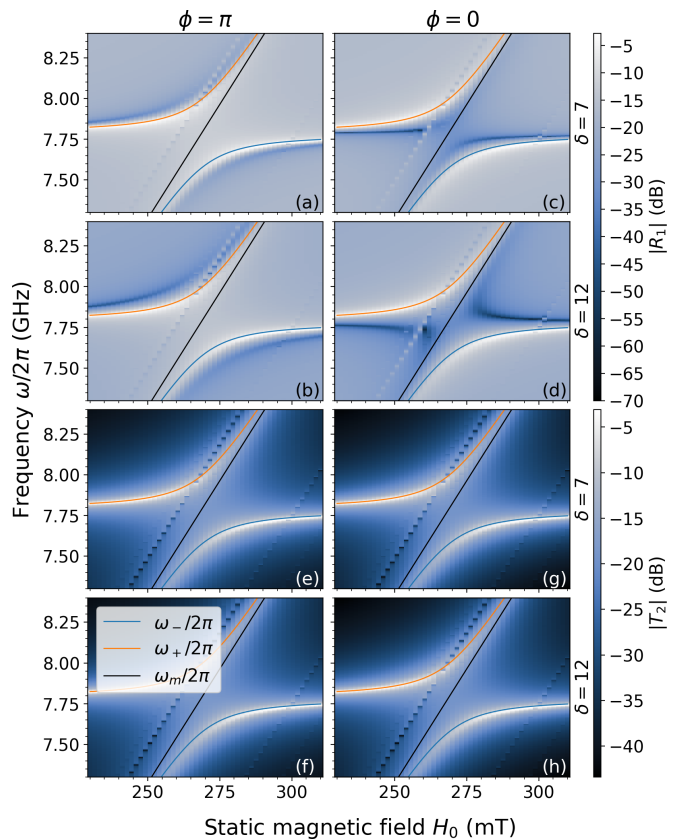


FIG. 4. Plots of the normalised reflection and transmission amplitudes  $|R_1|, |T_2|$  using the numerical values of the S parameters obtained using COMSOL. Note that contrary to fig. 2 we varied the amplitude  $\delta$  at Port 3 instead of the effective amplitude  $\delta_0$ , because the latter depends on the unknown parameters  $\kappa_1, \kappa_3$ .

magnon,  $\kappa_3/2\pi$  is maximum when  $\hat{\mathbf{n}} = \hat{\mathbf{y}}$ .

We first numerically calculated the S parameters for different values of  $\mathbf{H}_0$  using COMSOL [46]. From these two S parameters, we can plot  $R_1$  and  $T_2$  after normalising  $r_1(\omega) = S_{11} + \delta e^{i\phi} S_{13}$  and  $t_2(\omega) = S_{21} + \delta e^{i\phi} S_{23}$ , and we obtain the results of fig. 4, which successfully reproduce the input-output theory results of figs. 2 and 3. As a further verification, we also performed a fully two-tone experiment in COMSOL for  $\delta = 12$ , and the results were identical to those of the second and fourth rows of fig. 4.

*Effective Hamiltonian for the open system.* We have now confirmed that the resonances of  $R_1$  and  $T_2$  follow energy level repulsion, suggesting coherent coupling physics. However, one may worry that the physics of the two-tone driven system is different from the physics of the closed-system Hamiltonian of eq. (1), which not include the coherent drives. To derive the effective Hamiltonian, we write the QLEs eqs. (2) and (3) in the semi-classical approximation where operators are replaced by their expectation values. Recalling that  $\langle c^{\text{in}} \rangle = \langle m^{\text{in}} \rangle = 0$ , the

QLEs read

$$\dot{c} = -i\tilde{\omega}_c c - igm - \sqrt{\kappa_1} e^{i\phi_1} p_1^{\text{in}} - \sqrt{\kappa_2} e^{i\phi_2} p_2^{\text{in}}, \quad (14)$$

$$\dot{m} = -i\tilde{\omega}_m m - igc - \sqrt{\kappa_3} e^{i\phi_3} p_3^{\text{in}}, \quad (15)$$

In both a reflection and transmission measurement, port 2 is not driven, so we set  $p_2^{\text{in}} = 0$ . On the other hand,  $p_1^{\text{in}}$  and  $p_3^{\text{in}}$  correspond to a coherent drive at frequency  $\omega/2\pi$ , with amplitude  $\mathcal{E}$  and  $\delta e^{i\phi}\mathcal{E}$ . Thus, further defining  $\mathcal{E}_1 = \sqrt{\kappa_1/2\pi} e^{i\phi_1} \mathcal{E}$  and  $\mathcal{E}_3 = \sqrt{\kappa_3/2\pi} e^{i\phi_3} \mathcal{E} \delta e^{i\phi}$ , the QLEs become [42]

$$\dot{c} = -i\tilde{\omega}_c c - igm - \mathcal{E}_1 e^{-i\omega t}, \quad (16)$$

$$\dot{m} = -i\tilde{\omega}_m m - igc - \mathcal{E}_3 e^{-i\omega t} \quad (17)$$

From these equations, we find that the effective non-hermitian Hamiltonian (recall that  $\tilde{\omega}_c, \tilde{\omega}_m \in \mathbb{C}$ )

$$H_{\text{eff}} = \hbar\tilde{\omega}_c c^\dagger c + \hbar\tilde{\omega}_m m^\dagger m + \hbar(gcm^\dagger + g^*c^\dagger m) + i\hbar(\mathcal{E}_1 c e^{i\omega t} - \text{h.c.}) + i\hbar(\mathcal{E}_3 m e^{i\omega t} - \text{h.c.}) \quad (18)$$

where h.c stands for the hermitian conjugate terms, gives Heisenberg equations of motion identical to eqs. (16) and (17). Thus, the physics described by eq. (18) is identical to that given by the QLEs. After a rotating frame transformation to remove the time-dependence and displacement operations [47], this Hamiltonian is unitarily equivalent to

$$H'_{\text{eff}} = -\hbar\tilde{\Delta}_c c^\dagger c - \hbar\tilde{\Delta}_m m^\dagger m + \hbar(gcm^\dagger + g^*c^\dagger m). \quad (19)$$

*Physical interpretation and conclusion.* Formally similar to the closed-system Hamiltonian of eq. (1), this effective Hamiltonian describes the coherent coupling physics between photons and magnon, and thus its spectrum corresponds to level repulsion. Since  $H'_{\text{eff}}$  describes the physics of the cavity system in the presence of coherent drives, we conclude that the physics of two-tone driving indeed corresponds to coherent coupling, even though the reflection coefficient can show level attraction due to interference-based anti-resonances. Therefore, the anti-resonance frequencies  $\Omega_\pm/2\pi$  (dashed lines in fig. 2) do not correspond to the spectrum of the system, which are instead given by  $\omega_\pm/2\pi$  (solid lines in fig. 2).

It is worth noting that here, the anti-resonances leading to level attraction come from interferences between  $S_{11}$  and  $S_{13}$ . However, anti-resonances can also appear in a one-tone driven system as experimentally demonstrated by Rao *et al.* [48]. Notably, these anti-resonances can exhibit different coupling behaviour recently analysed by [41], and suggest energy level repulsion and attraction with a magnon mode. These behaviours are associated with the numerators of the transmission coefficient, and therefore they are not associated to a physical coherent and dissipative coupling. Importantly, it is incorrect to derive an effective Hamiltonian from this numerator alone, as it is not associated with a physical dynamics.

To conclude, we have showed that when two bosonic modes are simultaneously driven, the resonances in reflection and transmission indeed inform on the normal modes of the system, while the observed anti-resonances are due to interference physics, and are unrelated to the coupled system. We note that while two-tone driving do not correspond to the in-situ control of coherent and dissipative couplings, achieving it is still a relevant research direction. Finally, we note that while we considered a cavity magnonics system as a physical realisation of two coupled bosonic modes, many other systems, such as intersubband polaritons [49] or cavity optomechanics in the red-detuned regime [50], reduce to a similar Hamiltonian. Indeed, the model Hamiltonian of eq. (1) is essentially the Dicke model [51] after employing the Holstein-Primakoff transformation [52] and then the rotating wave approximation [53]. Hence, the derivations employed here are very general and may prove useful to analyse the physics in other systems.

We acknowledge financial support from Thales Australia and Thales Research and Technology. The scientific colour map *oslo* [54] is used in this study to prevent visual distortion of the data and exclusion of readers with colourvision deficiencies [55]. This work is part of the research program supported by the European Union through the European Regional Development Fund (ERDF), by the Ministry of Higher Education and Research, Brittany and Rennes Métropole, through the CPER SpaceTech DroneTech, by Brest Métropole, and the ANR projects ICARUS (ANR-22-CE24-0008) and MagFunc (ANR-20-CE91-0005).

---

\* alan.gardin@adelaide.edu.au

- [1] L. Novotny, Strong coupling, energy splitting, and level crossings: A classical perspective, *American Journal of Physics* **78**, 1199 (2010).
- [2] C. Weisbuch, M. Nishioka, A. Ishikawa, and Y. Arakawa, Observation of the coupled exciton-photon mode splitting in a semiconductor quantum microcavity, *Physical Review Letters* **69**, 3314 (1992).
- [3] J. M. Dobrindt, I. Wilson-Rae, and T. J. Kippenberg, Parametric normal-mode splitting in cavity optomechanics, *Physical Review Letters* **101**, 263602 (2008).
- [4] N. Gisin and R. Thew, Quantum communication, *Nature Photonics* **1**, 165 (2007).
- [5] H. J. Kimble, The quantum internet, *Nature* **453**, 1023 (2008).
- [6] D. Lachance-Quirion, Y. Tabuchi, A. Gloppe, K. Usami, and Y. Nakamura, Hybrid quantum systems based on magnonics, *Applied Physics Express* **12**, 070101 (2019).
- [7] C. Lu, B. Turner, Y. Gui, J. Burgess, J. Xiao, and C.-M. Hu, An experimental demonstration of level attraction with coupled pendulums, *American Journal of Physics* **91**, 585 (2023).
- [8] Y.-P. Wang and C.-M. Hu, Dissipative couplings in cavity magnonics, *Journal of Applied Physics* **127**, 130901

- (2020).
- [9] M. Harder, B. M. Yao, Y. S. Gui, and C.-M. Hu, Coherent and dissipative cavity magnonics, *Journal of Applied Physics* **129**, 201101 (2021).
- [10] Y.-P. Wang, J. Rao, Y. Yang, P.-C. Xu, Y. Gui, B. Yao, J. You, and C.-M. Hu, Nonreciprocity and unidirectional invisibility in cavity magnonics, *Physical Review Letters* **123**, 127202 (2019).
- [11] A. Metelmann and A. A. Clerk, Nonreciprocal photon transmission and amplification via reservoir engineering, *Physical Review X* **5**, 021025 (2015).
- [12] A. Clerk, Introduction to quantum non-reciprocal interactions: from non-hermitian hamiltonians to quantum master equations and quantum feedforward schemes, *SciPost Physics Lecture Notes* 10.21468/scipostphyslectnotes.44 (2022).
- [13] W. Yu, J. Wang, H. Yuan, and J. Xiao, Prediction of attractive level crossing via a dissipative mode, *Physical Review Letters* **123**, 227201 (2019).
- [14] B. Yao, T. Yu, Y. S. Gui, J. W. Rao, Y. T. Zhao, W. Lu, and C.-M. Hu, Coherent control of magnon radiative damping with local photon states, *Communications Physics* **2**, 10.1038/s42005-019-0264-z (2019).
- [15] B. Yao, T. Yu, X. Zhang, W. Lu, Y. Gui, C.-M. Hu, and Y. M. Blanter, The microscopic origin of magnon-photon level attraction by traveling waves: Theory and experiment, *Physical Review B* **100**, 214426 (2019).
- [16] O. Bleu, K. Choo, J. Levinsen, and M. M. Parish, Dissipative light-matter coupling and anomalous dispersion in nonideal cavities, *Physical Review A* **109**, 023707 (2024).
- [17] B. Kubala and J. König, Flux-dependent level attraction in double-dot aharonov-bohm interferometers, *Physical Review B* **65**, 245301 (2002).
- [18] W. D. Heiss, The physics of exceptional points, *Journal of Physics A: Mathematical and Theoretical* **45**, 444016 (2012).
- [19] D. Zhang, X.-Q. Luo, Y.-P. Wang, T.-F. Li, and J. Q. You, Observation of the exceptional point in cavity magnon-polaritons, *Nature Communications* **8**, 10.1038/s41467-017-01634-w (2017).
- [20] G.-Q. Zhang and J. Q. You, Higher-order exceptional point in a cavity magnonics system, *Physical Review B* **99**, 054404 (2019).
- [21] H. M. Hurst and B. Flebus, Non-hermitian physics in magnetic systems, *Journal of Applied Physics* **132**, 10.1063/5.0124841 (2022), arXiv:2209.03946 [cond-mat.mes-hall].
- [22] H. Xu, D. Mason, L. Jiang, and J. G. E. Harris, Topological energy transfer in an optomechanical system with exceptional points, *Nature* **537**, 80 (2016).
- [23] Y. Cao and P. Yan, Exceptional magnetic sensitivity of pt-symmetric cavity magnon polaritons, *Physical Review B* **99**, 214415 (2019).
- [24] T. Yu, H. Yang, L. Song, P. Yan, and Y. Cao, Higher-order exceptional points in ferromagnetic trilayers, *Physical Review B* **101**, 144414 (2020).
- [25] J. Koch, A. A. Houck, K. L. Hur, and S. M. Girvin, Time-reversal-symmetry breaking in circuit-QED-based photon lattices, *Physical Review A* **82**, 043811 (2010).
- [26] K. Sliwa, M. Hatridge, A. Narla, S. Shankar, L. Frunzio, R. Schoelkopf, and M. Devoret, Reconfigurable josephson circulator/directional amplifier, *Physical Review X* **5**, 041020 (2015).
- [27] K. Fang, J. Luo, A. Metelmann, M. H. Matheny, F. Marquardt, A. A. Clerk, and O. Painter, Generalized non-reciprocity in an optomechanical circuit via synthetic magnetism and reservoir engineering, *Nature Physics* **13**, 465 (2017).
- [28] X. Huang, C. Lu, C. Liang, H. Tao, and Y.-C. Liu, Loss-induced nonreciprocity, *Light: Science & Applications* **10**, 30 (2021).
- [29] I. Boventer, M. Kläui, R. Macêdo, and M. Weides, Steering between level repulsion and attraction: broad tunability of two-port driven cavity magnon-polaritons, *New Journal of Physics* **21**, 125001 (2019).
- [30] I. Boventer, C. Dörfinger, T. Wolz, R. Macêdo, R. Lebrun, M. Kläui, and M. Weides, Control of the coupling strength and linewidth of a cavity magnon-polariton, *Physical Review Research* **2**, 013154 (2020).
- [31] A. Bärnthaler, S. Rotter, F. Libisch, J. Burgdörfer, S. Gehler, U. Kuhl, and H.-J. Stöckmann, Probing decoherence through fano resonances, *Physical Review Letters* **105**, 056801 (2010).
- [32] M. F. Limonov, M. V. Rybin, A. N. Poddubny, and Y. S. Kivshar, Fano resonances in photonics, *Nature Photonics* **11**, 543 (2017).
- [33] Q. Lu, J. Guo, Y.-L. Zhang, Z. Fu, L. Chen, Y. Xiang, and S. Xie, Level attraction due to dissipative phonon-phonon coupling in an opto-mechano-fluidic resonator, *ACS Photonics* **10**, 699 (2023).
- [34] M. Khanbekyan, H. A. M. Leymann, C. Hopfmann, A. Foerster, C. Schneider, S. Höfling, M. Kamp, J. Wiersig, and S. Reitzenstein, Unconventional collective normal-mode coupling in quantum-dot-based bimodal microlasers, *Physical Review A* **91**, 043840 (2015).
- [35] N. R. Bernier, L. D. Tóth, A. K. Feofanov, and T. J. Kippenberg, Level attraction in a microwave optomechanical circuit, *Physical Review A* **98**, 023841 (2018).
- [36] N. R. Bernier, E. G. Dalla Torre, and E. Demler, Unstable avoided crossing in coupled spinor condensates, *Physical Review Letters* **113**, 065303 (2014).
- [37] C. W. Gardiner and M. J. Collett, Input and output in damped quantum systems: Quantum stochastic differential equations and the master equation, *Physical Review A* **31**, 3761 (1985).
- [38] J. Bourhill, V. Castel, A. Manchec, and G. Cochet, Universal characterization of cavity-magnon polariton coupling strength verified in modifiable microwave cavity, *Journal of Applied Physics* **128**, 073904 (2020).
- [39] G. Flower, M. Goryachev, J. Bourhill, and M. E. Tobar, Experimental implementations of cavity-magnon systems: from ultra strong coupling to applications in precision measurement, *New Journal of Physics* **21**, 095004 (2019).
- [40] A. Gardin, J. Bourhill, V. Vlaminc, C. Person, C. Fumeaux, V. Castel, and G. C. Tettamanzi, Manifestation of the coupling phase in microwave cavity magnonics, *Physical Review Applied* **19**, 054069 (2023), arXiv:2212.05389 [quant-ph].
- [41] G. Bourcin, A. Gardin, J. Bourhill, V. Vlaminc, and V. Castel, Level attraction in a quasi-closed cavity, (2024), type: article, arxiv:2402.06258 [quant-ph].
- [42] See supplemental material at [url] for the derivation of the quantum langevin equation and the input-output theory.
- [43] See supplemental material at [url] for the expression of the transmission and its plot.
- [44] M. Goryachev, W. G. Farr, D. L. Creedon, Y. Fan,

- M. Kostylev, and M. E. Tobar, High-cooperativity cavity qed with magnons at microwave frequencies, *Phys. Rev. Applied* **2**, 054002 (2014).
- [45] N. Kostylev, M. Goryachev, and M. E. Tobar, Super-strong coupling of a microwave cavity to yttrium iron garnet magnons, *Applied Physics Letters* **108**, 062402 (2016).
- [46] See supplemental material at [url] for more details on the cavity used in the simulations and its characterisation.
- [47] See supplemental material at [url] for the details of the transformations.
- [48] J. W. Rao, C. H. Yu, Y. T. Zhao, Y. S. Gui, X. L. Fan, D. S. Xue, and C.-M. Hu, Level attraction and level repulsion of magnon coupled with a cavity anti-resonance, *New Journal of Physics* **21**, 065001 (2019).
- [49] C. Ciuti, G. Bastard, and I. Carusotto, Quantum vacuum properties of the intersubband cavity polariton field, *Physical Review B* **72**, 115303 (2005).
- [50] M. Aspelmeyer, T. J. Kippenberg, and F. Marquardt, Cavity optomechanics, *Reviews of Modern Physics* **86**, 1391 (2014).
- [51] K. Hepp and E. H. Lieb, On the superradiant phase transition for molecules in a quantized radiation field: the dicke maser model, *Annals of Physics* **76**, 360 (1973).
- [52] T. Holstein and H. Primakoff, Field dependence of the intrinsic domain magnetization of a ferromagnet, *Phys. Rev.* **58**, 1098 (1940).
- [53] A. Le Boité, Theoretical methods for ultra-strong light-matter interactions, *Advanced Quantum Technologies* **3**, 1900140 (2020), <https://onlinelibrary.wiley.com/doi/pdf/10.1002/qute.201900140>.
- [54] F. Crameri, Scientific colour maps (2021).
- [55] F. Crameri, G. E. Shephard, and P. J. Heron, The misuse of colour in science communication, *Nature Communications* **11**, 10.1038/s41467-020-19160-7 (2020).

# Supplementary information for “Level attraction from interference in two-tone driving”

Alan Gardin, Guillaume Bourcin, Christian Person, Christophe Fumeaux,  
Romain Lebrun, Isabella Boventer, Giuseppe C. Tettamanzi, and Vincent Castel

## CONTENTS

Derivation of the quantum Langevin equations	1
Calculation of the reflection at Port 1	3
Expression of the reflection at Port 1 with standard S-parameters	5
Calculation of the transmission	5
Expression of the reflection at Port 2 and the transmission at Port 1	6
Effective coupling strength and crosstalk	6
Simplification of the effective Hamiltonian	7
Finite element modelling results	8
References	11

## Derivation of the quantum Langevin equations

*System definition.* In this note, we derive the quantum Langevin equations of the coupled magnon/photon cavity system under the rotating wave approximation, which is valid for  $|g| \ll \omega_c, \omega_m$  [1, 2], where  $g/2\pi$  is the coupling strength. We recall that the most general Hamiltonian describing a coupled magnon-photon system reads [3]

$$H_{\text{sys}} = \hbar\omega_c c^\dagger c + \hbar\omega_m m^\dagger m + \hbar(gcm^\dagger + g^*c^\dagger m), \quad (1)$$

where  $g/2\pi$  is complex-valued due to potential coupling phases [4].

The intrinsic losses of the cavity and magnon modes (respectively due to radiative losses and the Gilbert damping) can be modelled by coupling to two bosonic baths described by the Hamiltonians

$$H_{\text{bath, intrinsic}} = \int_{\mathbb{R}} d\omega \hbar\omega a_\omega^\dagger a_\omega + \int_{\mathbb{R}} d\omega \hbar\omega b_\omega^\dagger b_\omega, \quad (2)$$

$$H_{\text{cav-bath, intrinsic}} = \int_{\mathbb{R}} d\omega i\hbar\sqrt{\frac{\kappa_c}{2\pi}}(ca_\omega^\dagger - c^\dagger a_\omega) + \int_{\mathbb{R}} d\omega i\hbar\sqrt{\frac{\kappa_m}{2\pi}}(cb_\omega^\dagger - c^\dagger b_\omega). \quad (3)$$

Here, we have assumed frequency-independent (Markov approximation) and real-valued coupling rates  $\kappa_c/2\pi, \kappa_m/2\pi$  to the baths.

Additionally, the cavity system is coupled to the environment through three ports, used to inject and sense microwave fields. We label them as Port 1, Port 2, and Port 3. To model the coupling of the magnon and cavity modes to the ports, we again couple them to a bosonic bath, but this time we allow the coupling rates to be complex-valued to model potential dephasing of the microwaves through the coaxial cables or due to the antenna geometry [5]. Therefore, we assume that the cavity mode couples to Ports 1 and 2 with coupling constants  $\kappa_1/2\pi, \kappa_2/2\pi$ , and phases  $\phi_1, \phi_2$ , while the magnon couples to Port 3 only, with coupling constant  $\kappa_3/2\pi$  and phase  $\phi_3$ . For the sake of completeness, we further consider that the cavity mode can couple to Port 3 with coupling constant  $\zeta\kappa_3/2\pi$  and phase  $\phi'_3$ , where  $\zeta$

a dimensionless constant. The continuous-frequency bosonic bath of port  $i$  is described by creation and annihilation operators  $p_{i,\omega}^\dagger, p_{i,\omega}$  with Hamiltonian

$$H_{\text{bath,ports}} = \sum_{i=1}^3 \int_{\mathbb{R}} d\omega \hbar \omega p_{i,\omega}^\dagger p_{i,\omega}. \quad (4)$$

while the interaction between the bath and the cavity system is modelled by

$$\begin{aligned} H_{\text{cav-bath,ports}} = & \int_{\mathbb{R}} d\omega i\hbar \sqrt{\frac{\kappa_1}{2\pi}} \left( c p_{1,\omega}^\dagger e^{-i\phi_1} - c^\dagger p_{1,\omega} e^{i\phi_1} \right) + \int_{\mathbb{R}} d\omega i\hbar \sqrt{\frac{\kappa_2}{2\pi}} \left( c p_{2,\omega}^\dagger e^{-i\phi_2} - c^\dagger p_{2,\omega} e^{i\phi_2} \right) \\ & + \int_{\mathbb{R}} d\omega i\hbar \sqrt{\frac{\kappa_3}{2\pi}} \left( m p_{3,\omega}^\dagger e^{-i\phi_3} - m^\dagger p_{3,\omega} e^{i\phi_3} \right) + \int_{\mathbb{R}} d\omega i\hbar \sqrt{\frac{\zeta\kappa_3}{2\pi}} \left( c p_{3,\omega}^\dagger e^{-i\phi_3} - c^\dagger p_{3,\omega} e^{i\phi_3'} \right). \end{aligned} \quad (5)$$

Thus, the total Hamiltonian of the joint cavity system and environment is

$$H = H_{\text{sys}} + H_{\text{bath,intrinsic}} + H_{\text{cav-bath,intrinsic}} + H_{\text{bath,ports}} + H_{\text{cav-bath,ports}}. \quad (6)$$

*Equation of motions.* The Heisenberg equation of motion for  $p_{1,\omega}$  is

$$\dot{p}_{1,\omega}(t) = -i\omega p_{1,\omega}(t) + \sqrt{\frac{\kappa_1}{2\pi}} e^{-i\phi_1} c(t). \quad (7)$$

The formal solution for an arbitrary  $t_0 < t$  is

$$p_{1,\omega}(t) = e^{-i\omega(t-t_0)} p_{1,\omega}(t_0) + \int_{t_0}^t dt' \sqrt{\frac{\kappa_1}{2\pi}} e^{-i\phi_1} c(t') e^{-i\omega(t-t')}, \quad (8)$$

and by analogy we deduce that

$$p_{2,\omega}(t) = e^{-i\omega(t-t_0)} p_{2,\omega}(t_0) + \int_{t_0}^t dt' \sqrt{\frac{\kappa_2}{2\pi}} e^{-i\phi_2} c(t') e^{-i\omega(t-t')}, \quad (9)$$

$$p_{3,\omega}(t) = e^{-i\omega(t-t_0)} p_{3,\omega}(t_0) + \int_{t_0}^t dt' \sqrt{\frac{\kappa_3}{2\pi}} e^{-i\phi_3} m(t') e^{-i\omega(t-t')} + \int_{t_0}^t dt' \sqrt{\frac{\zeta\kappa_3}{2\pi}} e^{-i\phi_3'} c(t') e^{-i\omega(t-t')}, \quad (10)$$

$$a_\omega(t) = e^{-i\omega(t-t_0)} a_\omega(t_0) + \int_{t_0}^t dt' \sqrt{\frac{\kappa_c}{2\pi}} c(t') e^{-i\omega(t-t')}, \quad (11)$$

$$b_\omega(t) = e^{-i\omega(t-t_0)} b_\omega(t_0) + \int_{t_0}^t dt' \sqrt{\frac{\kappa_m}{2\pi}} m(t') e^{-i\omega(t-t')}. \quad (12)$$

Taking  $t_0 \rightarrow -\infty$  and using  $\int_{-\infty}^t dt' f(t') \delta(t-t') = \frac{1}{2} f(t)$ , the Heisenberg equation of motion for  $m$  is

$$\dot{m}(t) = -i\omega_m m(t) - igc(t) - \sqrt{\frac{\kappa_m}{2\pi}} \int_{\mathbb{R}} d\omega b_\omega(t) - \sqrt{\frac{\kappa_3}{2\pi}} e^{i\phi_3} \int_{\mathbb{R}} d\omega p_{3,\omega}(t) \quad (13)$$

$$\begin{aligned} &= -i\omega_m m(t) - igc(t) - \sqrt{\kappa_m} m^{\text{in}}(t) - \frac{\kappa_m}{2\pi} \int_{t_0 \rightarrow -\infty}^t dt' m(t') \int_{\mathbb{R}} d\omega e^{-i\omega(t-t')} \\ &\quad - \sqrt{\kappa_3} e^{i\phi_3} p_3^{\text{in}}(t) - \frac{\kappa_3}{2\pi} \int_{t_0 \rightarrow -\infty}^t dt' \left( m(t') + e^{i(\phi_3 - \phi_3')} \sqrt{\zeta} c(t') \right) 2\pi \delta(t-t') \end{aligned} \quad (14)$$

$$= -i\tilde{\omega}_m m(t) - \left( ig + e^{i(\phi_3 - \phi_3')} \sqrt{\zeta} \frac{\kappa_3}{2} \right) c(t) - \sqrt{\kappa_m} m^{\text{in}}(t) - \sqrt{\kappa_3} e^{i\phi_3} p_3^{\text{in}}(t), \quad (15)$$

with  $\tilde{\omega}_m = \omega_m - i \frac{\kappa_m + \kappa_3}{2}$ ,

$$p_i^{\text{in}}(t) = \lim_{t_0 \rightarrow -\infty} \frac{1}{\sqrt{2\pi}} \int_{\mathbb{R}} d\omega e^{-i\omega(t-t_0)} p_{i,\omega}(t_0), \quad (16)$$

and

$$c^{\text{in}}(t) = \lim_{t_0 \rightarrow -\infty} \frac{1}{\sqrt{2\pi}} \int_{\mathbb{R}} d\omega e^{-i\omega(t-t_0)} a_\omega(t_0), \quad m^{\text{in}}(t) = \lim_{t_0 \rightarrow -\infty} \frac{1}{\sqrt{2\pi}} \int_{\mathbb{R}} d\omega e^{-i\omega(t-t_0)} b_\omega(t_0). \quad (17)$$

Similarly, the Heisenberg equation of motion for  $c$  reads

$$\begin{aligned} \dot{c}(t) &= -i\omega_c c(t) - ig^* m(t) - \sqrt{\frac{\kappa_c}{2\pi}} \int_{\mathbb{R}} d\omega a_\omega(t) \\ &\quad - \sqrt{\frac{\kappa_1}{2\pi}} e^{i\phi_1} \int_{\mathbb{R}} d\omega p_{1,\omega}(t) - \sqrt{\frac{\kappa_2}{2\pi}} e^{i\phi_2} \int_{\mathbb{R}} d\omega p_{2,\omega}(t) - \sqrt{\frac{\zeta\kappa_3}{2\pi}} e^{i\phi'_3} \int_{\mathbb{R}} d\omega p_{3,\omega}(t) \end{aligned} \quad (18)$$

$$\begin{aligned} &= -i\omega_c c(t) - ig^* m(t) - e^{i(\phi'_3 - \phi_3)} \sqrt{\zeta \frac{\kappa_3}{2}} m(t) - \frac{\kappa_c + \kappa_1 + \kappa_2 + \zeta\kappa_3}{2} c(t) \\ &\quad - \sqrt{\kappa_c} c^{\text{in}}(t) - \sqrt{\kappa_1} e^{i\phi_1} p_1^{\text{in}}(t) - \sqrt{\kappa_2} e^{i\phi_2} p_2^{\text{in}}(t) - \sqrt{\zeta\kappa_3} e^{i\phi'_3} p_3^{\text{in}}(t) \end{aligned} \quad (19)$$

$$= -i\tilde{\omega}_c c(t) - \tilde{g}' m(t) - \sqrt{\kappa_c} c^{\text{in}}(t) - \sqrt{\kappa_1} e^{i\phi_1} p_1^{\text{in}}(t) - \sqrt{\kappa_2} e^{i\phi_2} p_2^{\text{in}}(t) - \sqrt{\zeta\kappa_3} e^{i\phi'_3} p_3^{\text{in}}(t). \quad (20)$$

where we defined  $\tilde{\omega}_c = \omega_c - i\frac{\kappa_c + \kappa_1 + \kappa_2 + \zeta\kappa_3}{2}$  and  $\tilde{g}' = g^* - i\sqrt{\zeta \frac{\kappa_3}{2}} e^{i(\phi'_3 - \phi_3)}$ . Similarly defining  $\tilde{g} = g - i\sqrt{\zeta \frac{\kappa_3}{2}} e^{i(\phi_3 - \phi'_3)}$ , we can rewrite the Heisenberg equation of motions as

$$\dot{m} = -i\tilde{\omega}_m m - \tilde{g}c - \sqrt{\kappa_m} m^{\text{in}}(t) - \sqrt{\kappa_3} e^{i\phi_3} p_3^{\text{in}}(t), \quad (21)$$

$$\dot{c} = -i\tilde{\omega}_c c - i\tilde{g}' m - \sqrt{\kappa_c} c^{\text{in}}(t) - \sqrt{\kappa_1} e^{i\phi_1} p_1^{\text{in}}(t) - \sqrt{\kappa_2} e^{i\phi_2} p_2^{\text{in}}(t) - \sqrt{\zeta\kappa_3} e^{i\phi'_3} p_3^{\text{in}}(t), \quad (22)$$

which are the QLEs given in the main text.

### Calculation of the reflection at Port 1

*Frequency-space solutions.* We now perform a semi-classical approximation, and replace operators by their expectation value. Recalling that  $\langle c^{\text{in}} \rangle = \langle m^{\text{in}} \rangle = 0$ , the QLEs simplify to

$$\dot{m} = -i\tilde{\omega}_m m - i\tilde{g}c - \sqrt{\kappa_3} e^{i\phi_3} p_3^{\text{in}}(t), \quad (23)$$

$$\dot{c} = -i\tilde{\omega}_c c - i\tilde{g}' m - \sqrt{\kappa_1} e^{i\phi_1} p_1^{\text{in}}(t) - \sqrt{\kappa_2} e^{i\phi_2} p_2^{\text{in}}(t) - \sqrt{\zeta\kappa_3} e^{i\phi'_3} p_3^{\text{in}}(t), \quad (24)$$

and in frequency space,

$$-i\omega \tilde{m} = -i\tilde{\omega}_m \tilde{m} - i\tilde{g}\tilde{c} - \sqrt{\kappa_3} e^{i\phi_3} \tilde{p}_3^{\text{in}}, \quad (25)$$

$$-i\tilde{\Delta}_c \tilde{c} = -i\tilde{g}' \tilde{m} - \sqrt{\kappa_1} e^{i\phi_1} \tilde{p}_1^{\text{in}} - \sqrt{\kappa_2} e^{i\phi_2} \tilde{p}_2^{\text{in}} - \sqrt{\zeta\kappa_3} e^{i\phi'_3} \tilde{p}_3^{\text{in}}, \quad (26)$$

with  $\tilde{\Delta}_c = \omega - \tilde{\omega}_c$  and  $\tilde{\Delta}_m = \omega - \tilde{\omega}_m$ . In particular, the first equation gives

$$\tilde{m} = \frac{\tilde{g}\tilde{c} - i\sqrt{\kappa_3} e^{i\phi_3} \tilde{p}_3^{\text{in}}}{\tilde{\Delta}_m}, \quad (27)$$

which inserted in the second equation leads to

$$\tilde{c} = \frac{\tilde{g}' \tilde{m} - i\sqrt{\kappa_1} e^{i\phi_1} \tilde{p}_1^{\text{in}} - i\sqrt{\kappa_2} e^{i\phi_2} \tilde{p}_2^{\text{in}} - i\sqrt{\zeta\kappa_3} e^{i\phi'_3} \tilde{p}_3^{\text{in}}}{\tilde{\Delta}_c} \quad (28)$$

$$\tilde{c} = \frac{-i}{A(\omega)} \left[ \tilde{\Delta}_m \sqrt{\kappa_1} e^{i\phi_1} \tilde{p}_1^{\text{in}} + \tilde{\Delta}_m \sqrt{\kappa_2} e^{i\phi_2} \tilde{p}_2^{\text{in}} + \left( \tilde{g}' e^{i\phi_3} + \sqrt{\zeta} e^{i\phi'_3} \tilde{\Delta}_m \right) \sqrt{\kappa_3} \tilde{p}_3^{\text{in}} \right] \quad (29)$$

where  $A(\omega) = \tilde{\Delta}_c \tilde{\Delta}_m - \tilde{g}\tilde{g}'$ .

*Input-output relations.* To derive the input-output relations, we first write the formal solution of  $p_{1,\omega}$  for  $t < t_1$  as

$$p_{1,\omega}(t) = e^{-i\omega(t-t_1)} p_{1,\omega}(t_1) - \int_t^{t_1} dt' \sqrt{\frac{\kappa_1}{2\pi}} e^{-i\phi_1} c(t') e^{-i\omega(t-t')}. \quad (30)$$

and we have on the one hand

$$\int_{\mathbb{R}} d\omega p_{1,\omega}(t) = \sqrt{2\pi} \left( p_1^{\text{in}}(t) + \frac{\sqrt{\kappa_1}}{2} e^{-i\phi_1} c(t) \right), \quad (31)$$

and on the other

$$\int_{\mathbb{R}} d\omega p_{1,\omega}(t) = \sqrt{2\pi} \left( p_{1,\omega}^{\text{out}}(t) - \frac{\sqrt{\kappa_1}}{2} e^{-i\phi_1} c(t) \right), \quad (32)$$

so that the input-output relation is

$$p_1^{\text{out}}(t) = p_1^{\text{in}}(t) + \sqrt{\kappa_1} e^{-i\phi_1} c(t). \quad (33)$$

We can similarly derive

$$p_2^{\text{out}}(t) = p_2^{\text{in}}(t) + \sqrt{\kappa_2} e^{-i\phi_2} c(t), \quad (34)$$

$$p_3^{\text{out}}(t) = p_3^{\text{in}}(t) + \sqrt{\kappa_3} e^{-i\phi_3} m(t) + \sqrt{\zeta \kappa_3} e^{-i\phi_3'} c(t). \quad (35)$$

*Modelling coherent drives.* To examine the reflection and transmission, we consider that  $p_1$ , coupling to the cavity mode, is a coherent drive at frequency  $\omega_d/2\pi$ . Such a coherent drive is expected to reproduce the classical dynamics through the use of coherent states [6]. Formally, the state space for  $p_1$  is the product of the Fock space of the bath operators  $p_{1,\omega}$  for each frequency  $\omega/2\pi$ . Formally, the state of the bath is the tensor product  $\bigotimes_{\omega \in \mathbb{R}} |\psi_\omega\rangle$ , where  $|\psi_\omega\rangle$  is the state of the bosonic mode described by the annihilation operator  $p_{1,\omega}$ . If we assume a coherent drive, then only the mode of frequency  $\omega_d/2\pi$  has a non-vanishing number of excitation, which we take to be a coherent state  $|\mathcal{E}_{\omega_d}\rangle$ . Formally,  $|\psi_\omega\rangle = |0\rangle$  if  $\omega \neq \omega_d$ , and  $|\psi_\omega\rangle = |\mathcal{E}_{\omega_d}\rangle$  if  $\omega = \omega_d$ . Hence,  $\langle p_1 \rangle = \langle \mathcal{E}_{\omega_d} | p_1 | \mathcal{E}_{\omega_d} \rangle = \mathcal{E}_{\omega_d} \in \mathbb{C}$ , since we recall that coherent states are eigenstates of annihilation operators [6]. We make a similar approximation for Port 3 driving the magnon, albeit with a different amplitude and phase, and hence  $\langle p_3 \rangle = \delta e^{i\phi} \mathcal{E}_{\omega_d}$ .

A convenient choice for the coherent state  $\mathcal{E}_{\omega_d}$  is  $\mathcal{E}_{\omega_d} = \lim_{t_0 \rightarrow -\infty} \alpha e^{-i\omega_d t_0}$  with  $\mathcal{E} \in \mathbb{R}$ . Indeed, in the time-domain this gives for instance

$$\langle p_1^{\text{in}}(t) \rangle = \langle \mathcal{E}_{\omega_d} | p_1^{\text{in}}(t) | \mathcal{E}_{\omega_d} \rangle \quad (36)$$

$$= \lim_{t_0 \rightarrow -\infty} \langle \alpha e^{i\omega_d t_0} | \frac{1}{\sqrt{2\pi}} \int_{\mathbb{R}} d\omega e^{-i\omega(t-t_0)} p_{1,\omega}(t_0) | \mathcal{E} e^{-i\omega_d t_0} \rangle \quad (37)$$

$$= \lim_{t_0 \rightarrow -\infty} \langle \mathcal{E} e^{i\omega_d t_0} | \frac{1}{\sqrt{2\pi}} e^{-i\omega_d(t-t_0)} \alpha e^{-i\omega_d t_0} | \mathcal{E} e^{-i\omega_d t_0} \rangle \quad (38)$$

$$= \frac{\mathcal{E}}{\sqrt{2\pi}} e^{-i\omega_d t} \quad (39)$$

where in the third line we used the fact that a coherent state is an eigenstate of the annihilation operator, and that  $p_{1,\omega} | \mathcal{E} e^{-i\omega_d t_0} \rangle = 0$  if  $\omega \neq \omega_d$ .

*Expression of the reflection coefficient.* From  $\langle p_1^{\text{in}}(t) \rangle = \frac{\mathcal{E}}{\sqrt{2\pi}} e^{-i\omega_d t}$ , we see that  $\langle \tilde{p}_1^{\text{in}}(\omega) \rangle = \mathcal{E} \delta(\omega - \omega_d)$ . Thus, assimilating  $\omega$  to the frequency of the drive, the reflection at Port 1 reads

$$r_1(\omega) = \left. \frac{\tilde{p}_1^{\text{out}}}{\tilde{p}_1^{\text{in}}} \right|_{\tilde{p}_2^{\text{in}}=0} = 1 + \sqrt{\kappa_1} e^{-i\phi_1} \frac{\tilde{c}|_{\tilde{p}_2^{\text{in}}=0}}{\tilde{p}_1^{\text{in}}} \quad (40)$$

$$= 1 - i\sqrt{\kappa_1} \frac{\tilde{\Delta}_m \sqrt{\kappa_1}}{A(\omega)} - i\sqrt{\kappa_1} e^{-i\phi_1} \frac{(\tilde{g}' e^{i\phi_3} + \sqrt{\zeta} e^{i\phi_3'} \tilde{\Delta}_m) \sqrt{\kappa_3} \tilde{p}_3^{\text{in}}}{A(\omega) \tilde{p}_1^{\text{in}}} \quad (41)$$

$$= 1 - i\sqrt{\kappa_1} \frac{\tilde{\Delta}_m \sqrt{\kappa_1} + (\tilde{g}' e^{i(\phi_3 - \phi_1)} + \sqrt{\zeta} e^{i(\phi_3' - \phi_1)} \tilde{\Delta}_m) \sqrt{\kappa_3} \delta e^{i\phi}}{A(\omega)} \quad (42)$$

Notice that for  $\kappa_3 = 0$ , i.e. only the cavity mode is driven, the expression for the reflection reduces to the  $S_{11}$  parameter.

*Normalisation.* For a standard coherent state  $|\mathcal{E}\rangle$ , the mean number of particle is given by  $|\mathcal{E}|^2$ . Here, the unit of the ports  $\langle p_k \rangle$  are  $\sqrt{\omega}$ , which can be seen by considering the quantum Langevin equations. Hence, for the ports,  $|\mathcal{E}|^2$  is a number of photons per second, which can be linked with the power of the drive  $P$  by

$$\mathcal{E} = \sqrt{\frac{P}{\hbar\omega_d}}. \quad (43)$$

Given that  $\langle p_3 \rangle = \delta e^{i\phi} \langle p_1 \rangle$ , we deduce that the power difference between Port 1 and Port 3 is given by  $\delta^2$ , which allows to renormalise the expression of the reflection and transmission.

### Expression of the reflection at Port 1 with standard S-parameters

In this note, we derive the expressions of the standard S-parameters, when only one port is active at a time. Assuming that port 3 is not active, i.e.  $\langle p_3^{\text{in}} \rangle = 0$  (which corresponds to  $\delta = 0$ ), the reflection  $r_1$  and transmission  $t_2$  coefficients of eqs. (42) and (50) reduce to

$$S_{11}(\omega) = 1 - i \frac{\tilde{\Delta}_m \kappa_1}{\tilde{\Delta}_c \tilde{\Delta}_m - \tilde{g}\tilde{g}'}, \quad (44)$$

$$S_{21}(\omega) = -i \frac{\tilde{\Delta}_m \sqrt{\kappa_1 \kappa_2} e^{i(\phi_1 - \phi_2)}}{\tilde{\Delta}_c \tilde{\Delta}_m - \tilde{g}\tilde{g}'}. \quad (45)$$

which are the standard S parameters for a two-port cavity. Note that by symmetry we also have

$$S_{12}(\omega) = -i \frac{\tilde{\Delta}_m \sqrt{\kappa_1 \kappa_2} e^{i(\phi_2 - \phi_1)}}{\tilde{\Delta}_c \tilde{\Delta}_m - \tilde{g}\tilde{g}'}, \quad S_{22}(\omega) = 1 - i \frac{\tilde{\Delta}_m \kappa_2}{\tilde{\Delta}_c \tilde{\Delta}_m - \tilde{g}\tilde{g}'}. \quad (46)$$

Similarly, using eq. (29) we find

$$S_{13}(\omega) = \left. \frac{\tilde{p}_1^{\text{out}}}{\tilde{p}_3^{\text{in}}} \right|_{\tilde{p}_1^{\text{in}} = \tilde{p}_2^{\text{in}} = 0} = \sqrt{\kappa_1} e^{-i\phi_1} \frac{\tilde{c} |_{\tilde{p}_1^{\text{in}} = \tilde{p}_2^{\text{in}} = 0}}{\tilde{p}_3^{\text{in}}} = -i \sqrt{\kappa_1 \kappa_3} \frac{\tilde{g}' e^{i(\phi_3 - \phi_1)} + \sqrt{\zeta} e^{i(\phi_3' - \phi_1)} \tilde{\Delta}_m}{A(\omega)}, \quad (47)$$

and hence

$$r_1(\omega) = S_{11} + \delta e^{i\phi} S_{13} = 1 - i \sqrt{\kappa_1} \frac{\tilde{\Delta}_m \sqrt{\kappa_1} + \left( \tilde{g}' e^{i(\phi_3 - \phi_1)} + \sqrt{\zeta} e^{i(\phi_3' - \phi_1)} \tilde{\Delta}_m \right) \sqrt{\kappa_3} \delta e^{i\phi}}{A(\omega)} \quad (48)$$

which matches with the equation given in the main text for  $\zeta = 0$ .

### Calculation of the transmission

Using the results of the input-output theory above, the transmission through Port 2 when Port 1 and 3 are active is calculated to be

$$t_2(\omega) = \left. \frac{\tilde{p}_2^{\text{out}}}{\tilde{p}_1^{\text{in}}} \right|_{\tilde{p}_2^{\text{in}} = 0} = \sqrt{\kappa_2} e^{-i\phi_2} \frac{\tilde{c} |_{\tilde{p}_2^{\text{in}} = 0}}{\tilde{p}_1^{\text{in}}} \quad (49)$$

$$= -i \sqrt{\kappa_2} \frac{\tilde{\Delta}_m \sqrt{\kappa_1} e^{i(\phi_1 - \phi_2)} + \left( \tilde{g}' e^{i(\phi_3 - \phi_2)} + \sqrt{\zeta} e^{i(\phi_3' - \phi_2)} \tilde{\Delta}_m \right) \sqrt{\kappa_3} \delta e^{i\phi}}{A(\omega)}. \quad (50)$$

Thus, the normalised transmission at Port 2 is  $T_2 = \frac{1}{\sqrt{1 + \delta^2}} t_2$ .

*Expression with S parameters.* Furthermore, from eq. (47), we see that  $S_{23}$  can be obtained from  $S_{13}$  by replacing  $(\kappa_1, \phi_1) \mapsto (\kappa_2, \phi_2)$ , and thus we have

$$S_{23}(\omega) = \left. \frac{\tilde{p}_2^{\text{out}}}{\tilde{p}_3^{\text{in}}} \right|_{\tilde{p}_1^{\text{in}} = \tilde{p}_2^{\text{in}} = 0} = \sqrt{\kappa_2} e^{-i\phi_2} \frac{\tilde{c} |_{\tilde{p}_1^{\text{in}} = \tilde{p}_2^{\text{in}} = 0}}{\tilde{p}_3^{\text{in}}} = -i \sqrt{\kappa_2 \kappa_3} \frac{\tilde{g}' e^{i(\phi_3 - \phi_2)} + \sqrt{\zeta} e^{i(\phi_3' - \phi_2)} \tilde{\Delta}_m}{A(\omega)}. \quad (51)$$

Hence, comparing eq. (50) with eqs. (45) and (51) we conclude that  $t_2 = S_{21} + \delta e^{i\phi} S_{23}$ .

*Zeros of the nominator.* The zeros of the nominator of  $T_2$  are given by

$$(\omega - \tilde{\omega}_m) \left[ \sqrt{\kappa_1} e^{i(\phi_1 - \phi_2)} + \sqrt{\zeta \kappa_3} e^{i(\phi_3' - \phi_2)} \delta e^{i\phi} \right] + \left( g^* - i \sqrt{\zeta} \frac{\kappa_3}{2} e^{i(\phi_3' - \phi_3)} \right) e^{i(\phi_3 - \phi_2)} \sqrt{\kappa_3} \delta e^{i\phi} = 0 \quad (52)$$

i.e.

$$\omega = \tilde{\omega}_m + \frac{\left( g^* - i \sqrt{\zeta} \frac{\kappa_3}{2} e^{i(\phi_3' - \phi_3)} \right) e^{i\phi_3} \sqrt{\kappa_3} \delta e^{i\phi}}{\sqrt{\kappa_1} e^{i\phi_1} + \sqrt{\zeta \kappa_3} e^{i\phi_3'} \delta e^{i\phi}}. \quad (53)$$

### Expression of the reflection at Port 2 and the transmission at Port 1

In the main text, we only consider that Port 1 is being driven, while Port 2 is passive and used as a probe. In this note, we exchange the role of Port 1 and Port 2 to check that the results are identical. Thus, we now have  $\langle p_2^{\text{in}}(t) \rangle = \frac{\mathcal{E}}{\sqrt{2\pi}} e^{-i\omega_d t}$ ,  $\langle p_3^{\text{in}} \rangle = \delta e^{i\phi} \langle p_1^{\text{in}} \rangle$ , and  $\langle p_2^{\text{in}} \rangle = 0$ . The reflection at Port 2 is

$$r_2(\omega) = \left. \frac{\tilde{p}_2^{\text{out}}}{\tilde{p}_2^{\text{in}}} \right|_{\tilde{p}_1^{\text{in}}=0} = 1 + \sqrt{\kappa_2} e^{-i\phi_2} \frac{\tilde{c}|_{\tilde{p}_1^{\text{in}}=0}}{\tilde{p}_2^{\text{in}}} \quad (54)$$

$$= 1 - i\sqrt{\kappa_2} \frac{\tilde{\Delta}_m \sqrt{\kappa_2} + \left( \tilde{g}' e^{i(\phi_3 - \phi_2)} + \sqrt{\zeta} e^{i(\phi'_3 - \phi_2)} \tilde{\Delta}_m \right) \sqrt{\kappa_3} \delta e^{i\phi}}{A(\omega)}, \quad (55)$$

and hence it is formally identical to  $r_1$  after replacing the index 1 by 2. For the transmission through Port 1,

$$t_1(\omega) = \left. \frac{\tilde{p}_1^{\text{out}}}{\tilde{p}_2^{\text{in}}} \right|_{\tilde{p}_1^{\text{in}}=0} = \sqrt{\kappa_1} e^{-i\phi_1} \frac{\tilde{c}|_{\tilde{p}_1^{\text{in}}=0}}{\tilde{p}_2^{\text{in}}} \quad (56)$$

$$= -i\sqrt{\kappa_1} \frac{\tilde{\Delta}_m \sqrt{\kappa_2} e^{i(\phi_2 - \phi_1)} + \left( \tilde{g}' e^{i(\phi_3 - \phi_1)} + \sqrt{\zeta} e^{i(\phi'_3 - \phi_1)} \tilde{\Delta}_m \right) \sqrt{\kappa_3} \delta e^{i\phi}}{A(\omega)}. \quad (57)$$

### Effective coupling strength and crosstalk

For non-vanishing coupling of Port 3 to the cavity mode,  $\zeta \neq 0$ , we recall that the reflection coefficient given by eq. (42) is

$$r_1(\omega) = \frac{N(\omega)}{D(\omega)} = 1 - i\sqrt{\kappa_1} \frac{\tilde{\Delta}_m \sqrt{\kappa_1} + \left( \tilde{g}' e^{i(\phi_3 - \phi_1)} + \sqrt{\zeta} e^{i(\phi'_3 - \phi_1)} \tilde{\Delta}_m \right) \sqrt{\kappa_3} \delta e^{i\phi}}{A(\omega)} \quad (58)$$

$$= \frac{\tilde{\Delta}_c \tilde{\Delta}_m - \tilde{g}\tilde{g}' - i\kappa_1 \tilde{\Delta}_m - i\tilde{g}' \sqrt{\kappa_1 \kappa_3} e^{i(\phi_3 - \phi_1)} \delta e^{i\phi} - i\tilde{\Delta}_m \sqrt{\zeta} \sqrt{\kappa_1 \kappa_3} e^{i(\phi'_3 - \phi_1)} \delta e^{i\phi}}{\tilde{\Delta}_c \tilde{\Delta}_m - \tilde{g}\tilde{g}'}. \quad (59)$$

The nominator is

$$N(\omega) = \omega^2 - (\tilde{\omega}_c + \tilde{\omega}_m)\omega + \tilde{\omega}_c \tilde{\omega}_m - \tilde{g}\tilde{g}' - i\kappa_1(\omega - \tilde{\omega}_m) - i\tilde{g}' \sqrt{\kappa_1 \kappa_3} \delta e^{i(\phi + \phi_3 - \phi_1)} - i(\omega - \tilde{\omega}_m) \sqrt{\zeta} \sqrt{\kappa_1 \kappa_3} \delta e^{i(\phi + \phi'_3 - \phi_1)} \quad (60)$$

$$= \omega^2 - \left( \tilde{\omega}_c + i \left[ \kappa_1 + \sqrt{\zeta} \sqrt{\kappa_1 \kappa_3} \delta e^{i(\phi + \phi'_3 - \phi_1)} \right] + \tilde{\omega}_m \right) \omega + \left( \tilde{\omega}_c + i \left[ \kappa_1 + \sqrt{\zeta} \sqrt{\kappa_1 \kappa_3} \delta e^{i(\phi + \phi'_3 - \phi_1)} \right] \right) \tilde{\omega}_m - \tilde{g}\tilde{g}' - i\tilde{g}' \sqrt{\kappa_1 \kappa_3} \delta e^{i(\phi + \phi_3 - \phi_1)} \quad (61)$$

$$= \omega^2 - (\tilde{\omega}_c'' + \tilde{\omega}_m)\omega + \tilde{\omega}_c'' \tilde{\omega}_m - \tilde{G}^2 \quad (62)$$

where  $\omega_c'' = \omega_c + i \left[ \kappa_1 + \sqrt{\zeta} \sqrt{\kappa_1 \kappa_3} \delta e^{i(\phi + \phi'_3 - \phi_1)} \right]$  and, recalling that  $g = |g| e^{i\varphi}$ ,

$$\tilde{G} = \sqrt{\tilde{g}\tilde{g}' + i\tilde{g}' \sqrt{\kappa_1 \kappa_3} \delta e^{i(\phi + \phi_3 - \phi_1)}} \quad (63)$$

$$= \sqrt{\left( g - i\sqrt{\zeta} e^{i(\phi_3 - \phi'_3)} \frac{\kappa_3}{2} \right) \left( g^* - i\sqrt{\zeta} e^{-i(\phi_3 - \phi'_3)} \frac{\kappa_3}{2} \right) + i \left( g^* - i\sqrt{\zeta} e^{-i(\phi_3 - \phi'_3)} \frac{\kappa_3}{2} \right) \sqrt{\kappa_1 \kappa_3} \delta e^{i(\phi + \phi_3 - \phi_1)}} \quad (64)$$

$$= |g| \sqrt{1 + \frac{\sqrt{\kappa_1 \kappa_3}}{|g|} \delta e^{i(\phi + \phi_3 - \phi_1 + \frac{\pi}{2} - \varphi)} - \frac{\sqrt{\zeta} \kappa_3}{|g|} \left( \frac{\sqrt{\zeta} \kappa_3}{4 |g|} + i \cos(\varphi + \phi'_3 - \phi_3) - \frac{\sqrt{\kappa_1 \kappa_3}}{2 |g|} \delta e^{i(\phi + \phi'_3 - \phi_1)} \right)}. \quad (65)$$

The first two terms under the square root correspond to the formula given in the main text, which corresponds to  $\zeta = 0$ . In fig. 1 we plot the reflection coefficient with parameters identical to those used in the main text, where  $\kappa_3/g = 1/2$ .

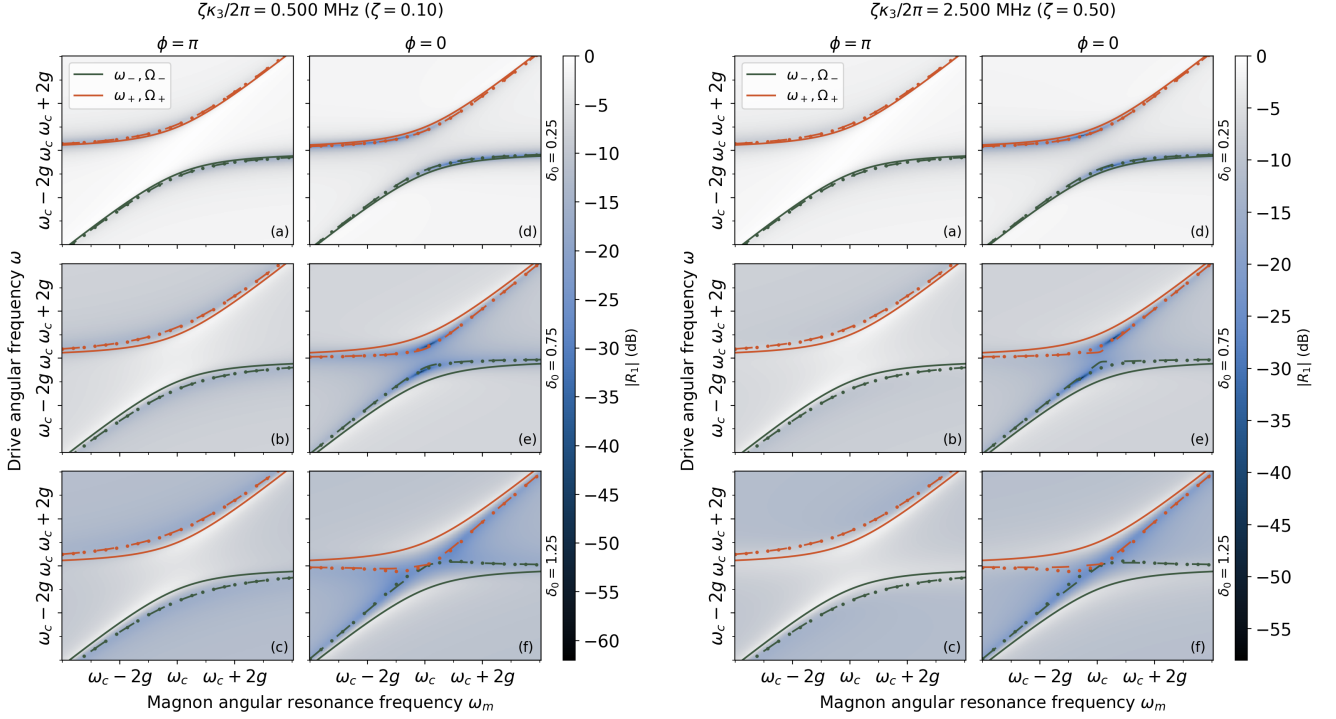


FIG. 1. Plot of the reflection amplitude  $|R_1|$  for  $\zeta = 0.1$  (left) and  $\zeta = 0.5$  (right), with other parameters as in figure 2 of the main text. The dashed lines corresponds to  $\zeta \neq 0$  (they are exactly the same as in figure 2 of the main text) while the dots corresponds to  $\zeta = 0$ .

### Simplification of the effective Hamiltonian

The effective Hamiltonian in the main text reads

$$H_{\text{eff}} = \hbar\tilde{\omega}_c c^\dagger c + \hbar\tilde{\omega}_m m^\dagger m + \hbar g(cm^\dagger + c^\dagger m) + i\hbar(\mathcal{E}_1 c e^{i\omega t} - \text{h.c.}) + i\hbar(\mathcal{E}_3 m e^{i\omega t} - \text{h.c.}). \quad (66)$$

To simplify the calculations, we define  $\epsilon_c = i\mathcal{E}_1$  and  $\epsilon_m = i\mathcal{E}_3$ , and we obtain

$$H_{\text{eff}} = \hbar\tilde{\omega}_c c^\dagger c + \hbar\tilde{\omega}_m m^\dagger m + \hbar g(cm^\dagger + c^\dagger m) + \hbar(\epsilon_c c e^{i\omega t} + \epsilon_c^* c^\dagger e^{-i\omega t}) + \hbar(\epsilon_m m e^{i\omega t} + \epsilon_m^* m^\dagger e^{-i\omega t}). \quad (67)$$

In a frame rotating with the drive, which corresponds to the unitary transformation  $U = \exp[i\omega_d t(c^\dagger c + m^\dagger m)]$ , we obtain

$$H_{\text{eff}} = \hbar\tilde{\Delta}_c c^\dagger c + \hbar\tilde{\Delta}_m m^\dagger m + \hbar g(cm^\dagger + c^\dagger m) + \hbar(\epsilon_c^* c + \epsilon_c c^\dagger) + \hbar(\epsilon_m^* m + \epsilon_m m^\dagger), \quad (68)$$

with the detunings  $\tilde{\Delta}_c = \tilde{\omega}_c - \omega_d$ ,  $\tilde{\Delta}_m = \tilde{\omega}_m - \omega_d$ .

Let us consider the driving terms as a perturbation  $V$ , and split the Hamiltonian of eq. (68) into  $H = H_0 + V$  where

$$H_0 = \hbar\Delta_c c^\dagger c + \hbar\Delta_m m^\dagger m + \hbar g(cm^\dagger + c^\dagger m), \quad (69)$$

$$V = \hbar(\epsilon_c c + \epsilon_c^* c^\dagger) + \hbar(\epsilon_m m + \epsilon_m^* m^\dagger). \quad (70)$$

We try to find a Schrieffer-Wolf transformation [7]  $U = e^\Lambda$  with  $\Lambda = (\lambda_c c - \lambda_c^* c^\dagger) + (\lambda_m m - \lambda_m^* m^\dagger)$ , and  $\lambda_c, \lambda_m$

constants to determine such that  $V + [\Lambda, H_0] = 0$ . Note that  $\Lambda^\dagger = -\Lambda$ , such that  $e^\Lambda$  is unitary. We have

$$\begin{aligned} V + [\Lambda, H_0] &= \epsilon_c c + \epsilon_c^* c^\dagger + \epsilon_m m + \epsilon_m^* m^\dagger \\ &\quad + [\lambda_c c - \lambda_c^* c^\dagger, \hbar \Delta_c c^\dagger c] + [\lambda_c c - \lambda_c^* c^\dagger, \hbar g (cm^\dagger + c^\dagger m)] \\ &\quad + [\lambda_m m - \lambda_m^* m^\dagger, \hbar \Delta_m m^\dagger m] + [\lambda_m m - \lambda_m^* m^\dagger, \hbar g (cm^\dagger + c^\dagger m)] \end{aligned} \quad (71)$$

$$\begin{aligned} &= \epsilon_c c + \epsilon_c^* c^\dagger + \epsilon_m m + \epsilon_m^* m^\dagger \\ &\quad + \hbar \Delta_c (\lambda_c c + \lambda_c^* c^\dagger) + \hbar g (\lambda_c m + \lambda_c^* m^\dagger) \\ &\quad + \hbar \Delta_m (\lambda_m m + \lambda_m^* m^\dagger) + \hbar g (\lambda_m c + \lambda_m^* c^\dagger) \end{aligned} \quad (72)$$

$$\begin{aligned} &= \hbar [(\epsilon_c + \Delta_c \lambda_c + g \lambda_m) c + (\epsilon_c^* + \Delta_c \lambda_c^* + g \lambda_m^*) c^\dagger] \\ &\quad + \hbar [(\epsilon_m + g \lambda_c + \Delta_m \lambda_m) m + (\epsilon_m^* + g \lambda_c^* + \Delta_m \lambda_m^*) m^\dagger]. \end{aligned} \quad (73)$$

Imposing  $V + [\Lambda, H_0] = 0$  (Schrieffer-Wolff condition) leads to

$$\begin{cases} \epsilon_c + \Delta_c \lambda_c + g \lambda_m = 0 \\ \epsilon_c^* + \Delta_c \lambda_c^* + g \lambda_m^* = 0 \\ \epsilon_m + g \lambda_c + \Delta_m \lambda_m = 0 \\ \epsilon_m^* + g \lambda_c^* + \Delta_m \lambda_m^* = 0 \end{cases}, \quad (74)$$

where we recognise that we get twice the same constraints by hermiticity. We can reduce the system to

$$\begin{cases} \epsilon_c + \Delta_c \lambda_c + g \lambda_m = 0 \\ \epsilon_m + g \lambda_c + \Delta_m \lambda_m = 0 \end{cases}, \quad \begin{cases} g \epsilon_c + g \Delta_c \lambda_c + g^2 \lambda_m = 0 \\ \Delta_c \epsilon_m + g \Delta_c \lambda_c + \Delta_c \Delta_m \lambda_m = 0 \end{cases}, \quad (75)$$

$$\begin{cases} \Delta_c \epsilon_m - g \epsilon_c + (\Delta_c \Delta_m - g^2) \lambda_m = 0 \\ g \lambda_c = -\epsilon_m - \Delta_m \lambda_m \end{cases}, \quad \begin{cases} \lambda_m = \frac{\Delta_c \epsilon_m - g \epsilon_c}{\Delta_c \Delta_m - g^2} \\ \lambda_c = -\frac{\epsilon_m}{g} - \frac{\Delta_m}{g} \frac{\Delta_c \epsilon_m - g \epsilon_c}{\Delta_c \Delta_m - g^2} \end{cases}. \quad (76)$$

The resulting Hamiltonian is

$$H' = H_0 + \frac{1}{2} [\Lambda, V] + \frac{1}{2} [\Lambda, [\Lambda, V]] + \mathcal{O}(\Lambda^3) \quad (77)$$

$$\begin{aligned} &= \hbar \Delta_c c^\dagger c + \hbar \Delta_m m^\dagger m + \hbar g (cm^\dagger + c^\dagger m) \\ &\quad + \frac{1}{2} [\lambda_c c - \lambda_c^* c^\dagger, \hbar (\epsilon_c c + \epsilon_c^* c^\dagger)] + \frac{1}{2} [\lambda_m m - \lambda_m^* m^\dagger, \hbar (\epsilon_m m + \epsilon_m^* m^\dagger)] \\ &= \hbar \Delta_c c^\dagger c + \hbar \Delta_m m^\dagger m + \hbar g (cm^\dagger + c^\dagger m) + \frac{\hbar}{2} (\lambda_c \epsilon_c^* + \lambda_c^* \epsilon_c + \lambda_m \epsilon_m^* + \lambda_m^* \epsilon_m). \end{aligned} \quad (78)$$

Note that the transformation is exact, since higher order commutators vanish (indeed, this is simply a displacement transformation). Furthermore, the last term is simply a constant energy offset with not physical effect, so it can be discarded.

The transformed Hamiltonian  $H'$  tells us that under coherent driving of both photons and magnons, the spectrum is equivalent to that of the undriven Hamiltonian  $H$  after the replacements  $(\omega_c, \omega_m \mapsto (\tilde{\omega}_c - \omega_d, \tilde{\omega}_m - \omega_d)$ , with  $\omega_d/2\pi$  the frequency of the drive. Hence, the standard level repulsion is obtained, and no level attraction can occur.

### Finite element modelling results

*Cavity design.* In this note, we detail the numerical results obtained using the RF module COMSOL Multiphysics<sup>®</sup> to simulate the two-tone driving experiment described by figure 1 in the main text. In the main text,  $p_1^{\text{in}}$  and  $p_3^{\text{in}}$  are defined as the signals output by the vector network analyser. Due to differing cable lengths or the geometry of the microwave probes, these signals can be dephased modelled using the phases  $\phi_1$  and  $\phi_3$ . To limit these effects as much as possible, we chose to use identical probes for Port 1 and Port 3. To that effect, the probe for Port 3 is inserted from the bottom of the cavity instead of on the side, as pictured in fig. 2.

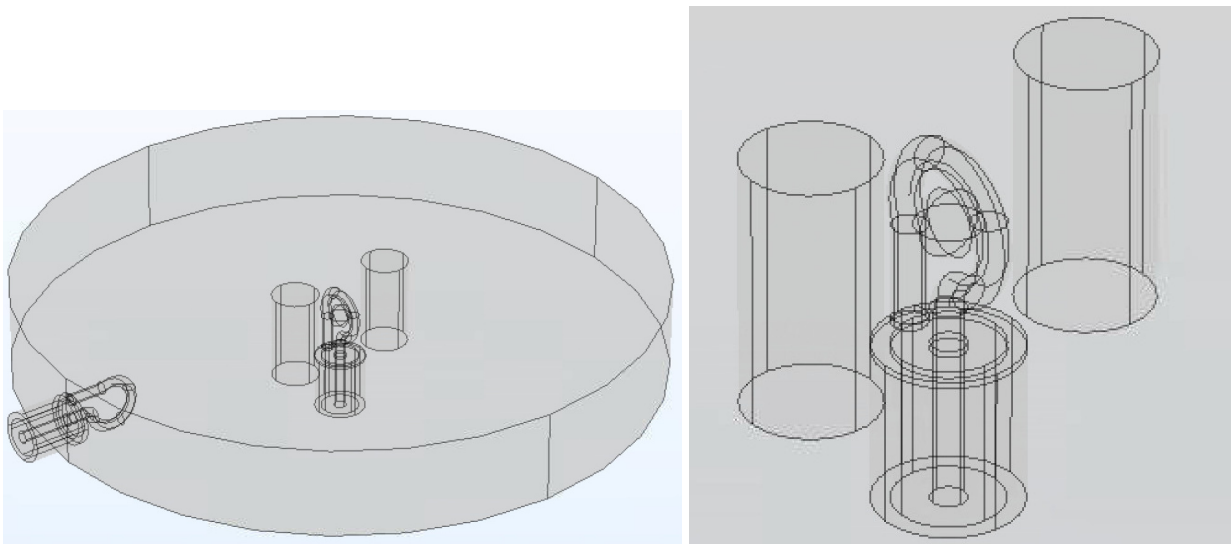


FIG. 2. Model of the two-post cavity we used in the COMSOL Multiphysics<sup>®</sup> simulations. The probes for Port 1 and Port 3 are an exact copy (dimensions and materials) limiting the effects of potential dephasings  $\phi_1$  and  $\phi_3$ .

*S parameters.* We first performed a frequency domain simulation to obtain the S-parameters of the cavity, shown in fig. 3. As expected, we observe energy level repulsion due to the coherent coupling of the photon and magnon in both reflection and transmission. Therefore, these simulations show that the physics of this system match with that predicted by the Hamiltonian model of equation (1) of the main text. We also note the presence of higher-order magnon modes corresponding to diagonal lines offset from the ferromagnetic frequency  $\omega_m/2\pi$ . This is especially the case for  $S_{33}$ , potentially due to the non-uniform magnetic field generated by the loop antenna.

*Estimation of  $\delta$  and  $\phi_0$ .* Next, we used the numerical values of  $S_{11}$  and  $S_{13}$  to compute and plot  $R_1 = S_{11} + \delta e^{i\phi} S_{13}$  for a range of  $\delta$  and  $\phi$ . The results, plotted in fig. 4, allow us to estimate very simply numerically which value of  $\delta$  and  $\phi$  are required to obtain level repulsion or attraction. We see that level repulsion and attraction are clearly visible for  $\delta = 12$  and  $\phi \in \{\pi, 0\}$  as predicted by the theory. This implies that the phase offset  $\phi_0 = \phi_1 - \phi_3 + \arg g - \frac{\pi}{2}$  in this system is  $\phi_0 = \pi$  since level repulsion is obtained when  $\phi - \phi_0 = \pi - \phi_0 = 0$ . Alternatively, one can extract the linewidths  $\kappa_1/2\pi, \kappa_3/2\pi$  and the coherent coupling  $|g|/2\pi$  from the S-parameters of fig. 3, and then use  $\delta_0 = \frac{\sqrt{\kappa_1 \kappa_3}}{|g|} \delta$  to estimate  $\delta$ . Then, one needs to sweep the dephasing  $\phi$  between the two drives to determine the phase offset  $\phi_0$ .

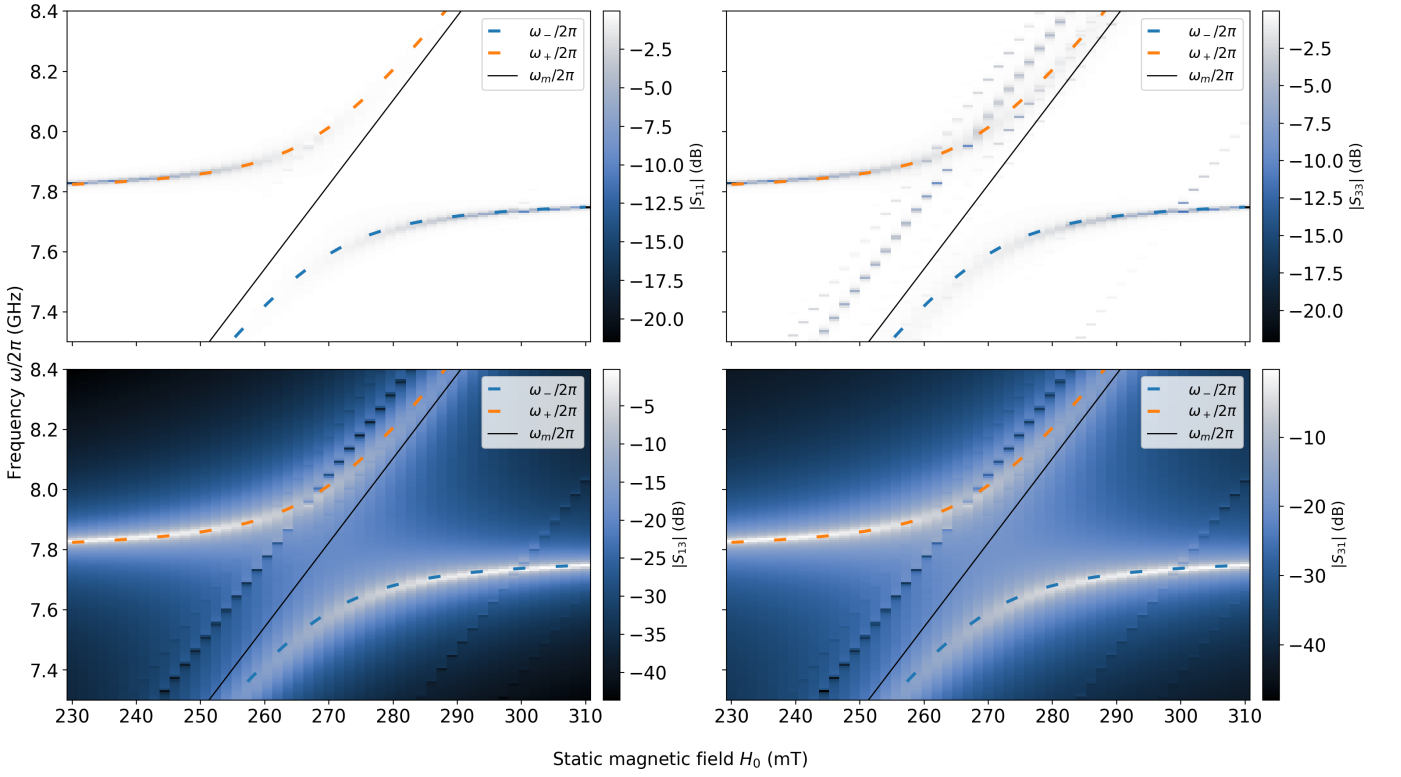


FIG. 3. Numerical calculations of the amplitude of the  $S$  parameters of the cavity. The polaritonic frequencies  $\omega_{\pm}/2\pi$  are given by equation (8) of the main text, and describe level repulsion, the signature of coherent coupling physics. The fit parameters are a coupling strength of  $g/2\pi = 210$  MHz and a cavity resonance at  $\omega_c/2\pi = 7.853$  GHz.

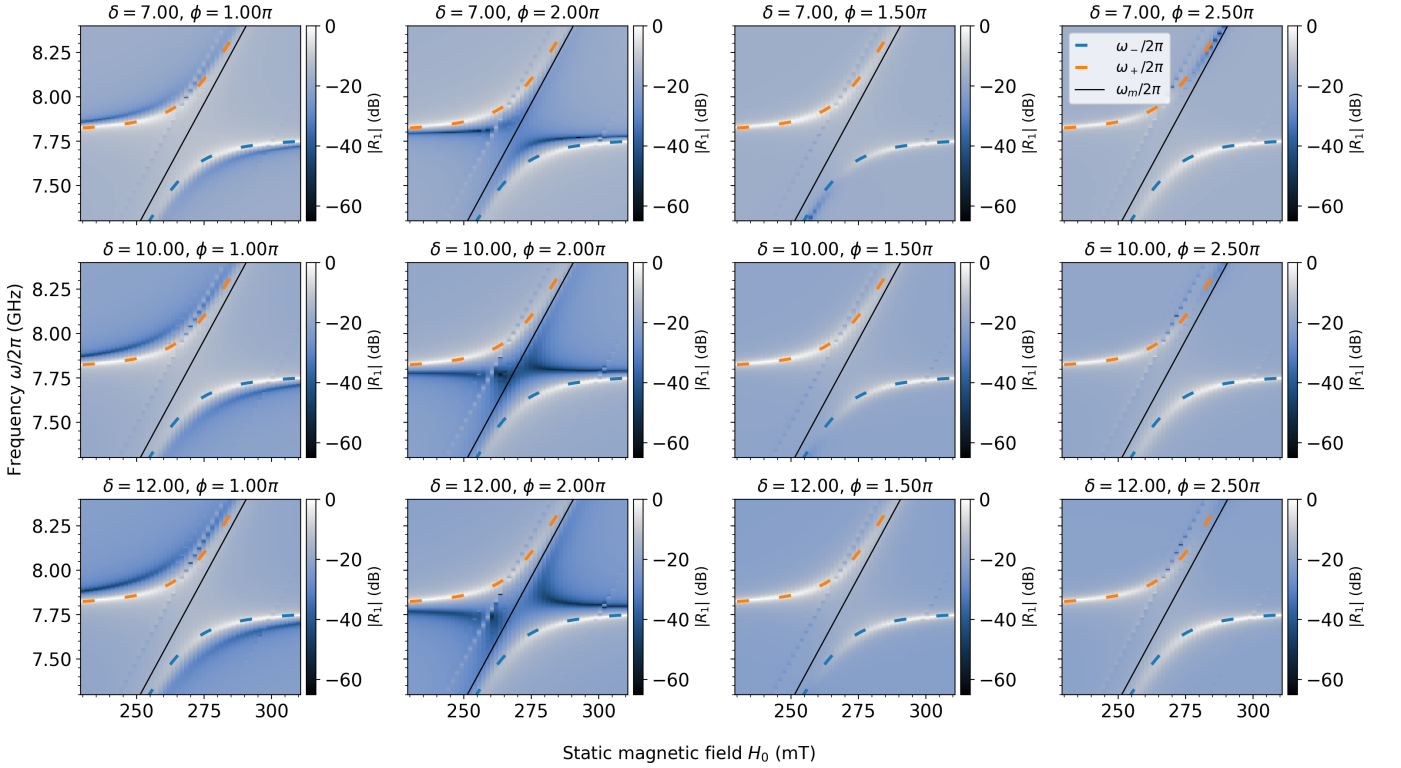


FIG. 4. Numerical calculations of the reflection  $R_1$  using the  $S$  parameters obtained using COMSOL Multiphysics<sup>®</sup>. The legend is common to all figures. The fit parameters are identical to this in fig. 3.

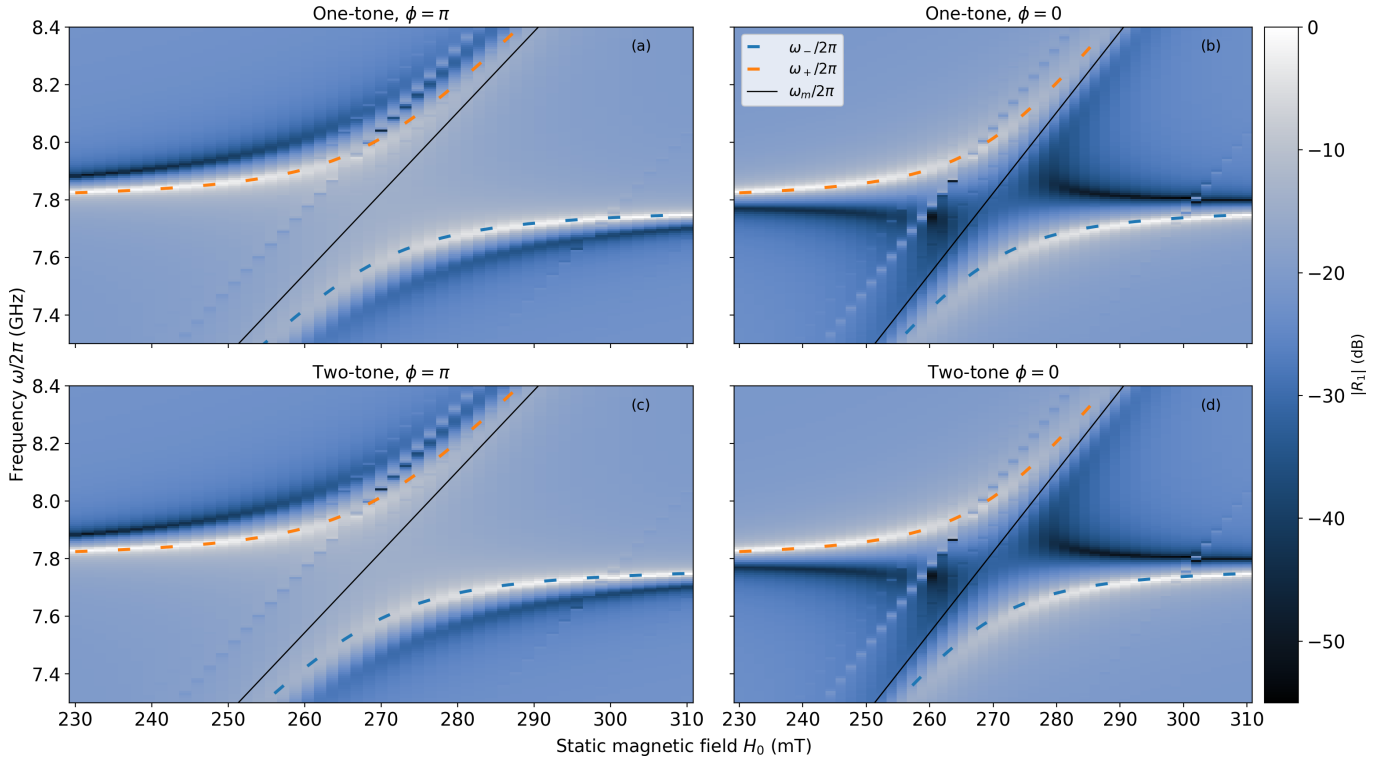


FIG. 5. Numerical calculations of the reflection at Port 1 with Port 3 active ( $R_1$ ) using COMSOL Multiphysics<sup>®</sup> for  $\delta = 12$ . (a-b) Evaluation of  $R_1$  from the S parameters using  $R_1 = S_{11} + \delta e^{i\phi} S_{13}$ . By definition of the S parameters, these are essentially a combination of one-tone simulations. (c-d) Fully two-tone simulation where both Port 1 and Port 3 are simultaneously active.

Having determined a suitable  $\delta$ , we can now perform a true two-tone driving experiment by enabling both Port 1 and Port 3 in COMSOL Multiphysics<sup>®</sup>. The results for  $\delta = 12$  (figs. 5(c) and 5(d)) are compared with the manual evaluation of  $R_1$  using the S parameters (figs. 5(a) and 5(b)). We observe a perfect agreement between the two.

- 
- [1] A. Frisk Kockum, A. Miranowicz, S. De Liberato, S. Savasta, and F. Nori, Ultrastrong coupling between light and matter, *Nature Reviews Physics* **1**, 19–40 (2019).
  - [2] A. Le Boité, Theoretical methods for ultrastrong light–matter interactions, *Advanced Quantum Technologies* **3**, 1900140 (2020), <https://onlinelibrary.wiley.com/doi/pdf/10.1002/qute.201900140>.
  - [3] G. Flower, M. Goryachev, J. Bourhill, and M. E. Tobar, Experimental implementations of cavity-magnon systems: from ultra strong coupling to applications in precision measurement, *New Journal of Physics* **21**, 095004 (2019).
  - [4] A. Gardin, J. Bourhill, V. Vlaminc, C. Person, C. Fumeaux, V. Castel, and G. C. Tettamanzi, Manifestation of the coupling phase in microwave cavity magnonics, *Physical Review Applied* **19**, 054069 (2023), arXiv:2212.05389 [quant-ph].
  - [5] G. Bourcin, A. Gardin, J. Bourhill, V. Vlaminc, and V. Castel, Level attraction in a quasi-closed cavity, (2024), type: article, arxiv:2402.06258 [quant-ph].
  - [6] M. Fox, *Quantum Optics: An Introduction*, Oxford Master Series in Physics (OUP Oxford, 2006).
  - [7] J. R. Schrieffer and P. A. Wolff, Relation between the anderson and kondo hamiltonians, *Physical Review* **149**, 491 (1966).